

Day - Night Effect Predictions for the SNO Detector

M. Maris^a and S.T. Petcov^{b,c)*}

a) *Osservatorio Astronomico di Trieste, I-34113 Trieste, Italy*

b) *Scuola Internazionale Superiore di Studi Avanzati, I-34014 Trieste, Italy*

c) *Istituto Nazionale di Fizica Nucleare, Sezione di Trieste, I-34014 Trieste, Italy*

Abstract

Detailed predictions for the day-night (D-N) asymmetry in the energy-integrated one year signals in the SNO detector in the case of the MSW $\nu_e \rightarrow \nu_{\mu(\tau)}$ and/or $\nu_e \rightarrow \nu_s$ transition solutions of the solar neutrino problem are presented. The asymmetries in the charged current (CC) and $\nu - e^-$ elastic scattering (ES) event rates are calculated for both MSW solutions; in the case of the $\nu_e \rightarrow \nu_s$ transition solution the D-N asymmetry in the neutral current (NC) event rate are derived as well. The asymmetries are calculated for three night samples of events which are produced by the solar neutrinos crossing i) the Earth mantle only (*Mantle*), ii) the Earth core (*Core*) and iii) the Earth core and/or the mantle (*Night*). The effects of the uncertainties i) in the values of the cross-sections of the CC and NC neutrino-induced reactions on deuterium, and ii) in the value of the bulk matter density and/or the chemical composition of the Earth core, on the corresponding D-N asymmetry predictions are analyzed. It is shown, in particular, that due to the strong enhancement of the transitions of the solar neutrinos crossing the Earth core, at $\sin^2 2\theta_V \leq 0.01$ the corresponding one year average D-N asymmetry in the *Core* sample of CC events in the case of the $\nu_e \rightarrow \nu_{\mu(\tau)}$ solution can be larger by a factor of up to ~ 8 than the asymmetry in the *Night* sample. In certain subregions of the MSW solution regions at small $\sin^2 2\theta_V$, the predicted magnitude of the *Core* D-N asymmetry in the CC sample is very sensitive to the value of the electron fraction number in the Earth core. Iso - (D-N) asymmetry contours in the $\Delta m^2 - \sin^2 2\theta_V$ plane for the SNO detector are derived in the region $\sin^2 2\theta_V \gtrsim 10^{-4}$ for the *Core* and *Night* samples of the CC, ES and NC

*Also at: Institute of Nuclear Research and Nuclear Energy, Bulgarian Academy of Sciences, BG-1784

events. The dependence of the D-N asymmetries considered on the final state e^- threshold energy in the CC and ES reactions is also investigated. Our results show, in particular, that the SNO experiment will be able to probe substantial parts of the SMA and LMA MSW $\nu_e \rightarrow \nu_{\mu(\tau)}$ solution regions by performing *Night* and *Core* D-N asymmetry measurements.

I. Introduction

In spite of the remarkable progress made in the studies of solar neutrinos the true cause of the solar neutrino deficit observed in the *Cl - Ar*, Kamiokande, *Ga - Ge*, and Super-Kamiokande experiments [1–5] is still not identified. The existing helioseismological data and its interpretation [6] make very unlikely the possibility of an astrophysical origin of the discrepancy between the solar neutrino observations [1–5] and the standard solar model predictions [7,8]. The hypotheses of vacuum oscillations or MSW transitions of solar neutrinos continue to provide viable solutions of the solar neutrino problem (see, e.g., [5,9–11]).

The current (mean event rate) solar neutrino data admit three types of MSW solutions if the solar ν_e undergo two-neutrino transitions into active neutrinos, $\nu_e \rightarrow \nu_{\mu(\tau)}$: the well-known small mixing angle (SMA) non-adiabatic and large mixing angle (LMA) adiabatic (see, e.g., [12,13]) and the so-called “LOW” solution (very recent analyses can be found in, e.g., [5,9–11]). While the SMA and LMA solutions have been shown to be rather stable with respect to variations in the values of the various physical quantities which enter into the calculations (the fluxes of ^8B and ^7Be neutrinos, nuclear reaction cross-sections, etc.), and of the data utilized in the analyses, the LOW solution is of the “borderline” type: its existence even at 99% C.L. is not stable with respect to relatively small changes in the data and/or in the relevant theoretical predictions (see, e.g., [9] and the references quoted therein.). To the three solutions there correspond three distinct regions in the plane of values of the two parameters, Δm^2 and $\sin^2 2\theta$, characterizing the transitions. One finds [5,9,11] using the standard solar model predictions [8] for the solar neutrino fluxes (^8B , ^7Be , pp , etc.) that at 99% C.L. the SMA MSW solution requires values in the intervals $4.0 \times 10^{-6} \text{ eV}^2 \lesssim \Delta m^2 \lesssim 10.0 \times 10^{-6} \text{ eV}^2$, $1.3 \times 10^{-3} \lesssim \sin^2 2\theta_V \lesssim 1.0 \times 10^{-2}$, the LMA solutions is realized for Δm^2 and $\sin^2 2\theta_V$ from the region $7.0 \times 10^{-6} \text{ eV}^2 \lesssim \Delta m^2 \lesssim 2.0 \times 10^{-4} \text{ eV}^2$, $0.50 \lesssim \sin^2 2\theta_V \lesssim 1.0$, and the LOW solution lies approximately in the region $0.4 \times 10^{-7} \text{ eV}^2 \lesssim \Delta m^2 \lesssim 1.5 \times 10^{-7} \text{ eV}^2$, $0.80 \lesssim \sin^2 2\theta_V \lesssim 1.0$. The SMA and LMA solution regions expand in the direction of smaller values of $\sin^2 2\theta_V$ up to $\sim 0.6 \times 10^{-3}$ and to ~ 0.3 , respectively, if one adopts more conservative approach in analyzing the data in terms of the MSW effect and treats the ^8B neutrino flux as a free parameter in the analysis (see, e.g., [11]). This enlargement of the two solution regions is not uniform in Δm^2 (see further). We will use the term “conservative” for the MSW solution regions derived by treating the ^8B neutrino flux as a free parameter.

The solar neutrino data can also be explained assuming that the solar neutrinos undergo MSW transitions into sterile neutrino in the Sun: $\nu_e \rightarrow \nu_s$ (see, e.g, [11,14]). In this case only a SMA solution is compatible with the data. The corresponding solution region obtained (at a given C.L.) using the mean event rate solar neutrino data and the predictions of ref. [8] for the different solar neutrino flux components practically coincides in magnitude and shape with the SMA $\nu_e \rightarrow \nu_{\mu(\tau)}$ solution region, but is shifted by a factor of ~ 1.2 along the Δm^2 axis to smaller values of Δm^2 . The “conservative” $\nu_e \rightarrow \nu_s$ transition solution region extends both in the direction of smaller and larger values of $\sin^2 2\theta_V$ down to 0.7×10^{-3} and up to 0.4 [11].

The results on the spectrum of the final state e^- from the $\nu - e^-$ elastic scattering reaction, obtained in the range of the recoil- e^- energy $E_e \sim (5 - 20)$ MeV by the Super-Kamiokande collaboration do not allow to rule out definitely any of the solutions of the solar neutrino problem indicated above [5]. The observed rise of the spectrum at $E_e \gtrsim 12$ MeV can be due to a contribution from the *hep* solar neutrinos [15], which complicates the interpretation of the data. The spectrum measured below 12 MeV is compatible with an energy-independent suppression of the ^8B neutrino flux, or with a mild energy dependence of the suppression.

A unique testable prediction of the MSW solutions of the solar neutrino problem is the day-night (D-N) effect - a difference between the solar neutrino event rates during the day and during the night,

caused by the additional transitions of the solar neutrinos taking place at night while the neutrinos cross the Earth on the way to the detector (see, e.g., [13,16,17] and the references quoted therein). The experimental observation of a non-zero D-N asymmetry

$$A_{D-N}^N \equiv \frac{R_N - R_D}{(R_N + R_D)/2}, \quad (1)$$

where R_N and R_D are, e.g., the one year averaged event rates in a given detector respectively during the night and the day, would be a very strong evidence in favor (if not a proof) of the MSW solution of the solar neutrino problem (see further).

Extensive predictions for the magnitude of the D-N effect for the Super-Kamiokande detector have been obtained in [18–22]. High precision calculations of the D-N asymmetry in the one year averaged recoil- e^- spectrum and in the energy-integrated event rates were performed for three event samples, *Night*, *Core* and *Mantle*, in [18–20]. The night fractions of these event samples are due to neutrinos which respectively cross the Earth along any trajectory, cross the Earth core, and cross only the Earth mantle (but not the core), on the way to the detector. The measurement of the D-N asymmetry in the *Core* sample was found to be of particular importance [18,19] because of the strong enhancement of the asymmetry, caused by a constructive interference between the amplitudes of the neutrino transitions in the Earth mantle and in the Earth core [23–25]. The effect differs from the MSW one [23]. The *mantle-core enhancement effect* is caused by the existence (for a given neutrino trajectory through the Earth core) of *points of resonance-like total neutrino conversion* in the corresponding space of neutrino oscillation parameters [24,25]. The location of these points determines the regions where the relevant probability of transitions in the Earth of the Earth-core-crossing solar neutrinos is large * [25]. At small mixing angles and in the case of $\nu_e \rightarrow \nu_{\mu(\tau)}$ transitions the predicted D-N asymmetry in the *Core* sample of the Super-Kamiokande data was shown [19] to be much bigger due to the *mantle-core enhancement effect* † - by a factor of up to ~ 6 , than the asymmetry in the *Night* sample. The asymmetry in the *Mantle* sample was found to be smaller than the asymmetry in the *Night* sample. On the basis of these results it was concluded in [19] that it can be possible to test a substantial part of the MSW $\nu_e \rightarrow \nu_{\mu(\tau)}$ SMA solution region in the $\Delta m^2 - \sin^2 2\theta_V$ plane by performing selective, i.e., *Core* D-N asymmetry measurements.

The current Super-Kamiokande data [5] shows a D-N asymmetry in the *Night* sample, which is different from zero at 1.9 s.d. level:

$$A_{D-N}^N = 0.065 \pm 0.031 \text{ (stat.)} \pm 0.013 \text{ (syst.)}. \quad (2)$$

These data do not allow to test the SMA solution region: the predicted asymmetry is too small (see, e.g., [19,21,22]). However, the Super-Kamiokande night data is given in 5 bins and 80% of the events in the bin N5 are due to Earth-core-crossing solar neutrinos [5], while the remaining 20% are produced by neutrinos which cross only the Earth mantle. Since the predicted D-N asymmetry in the *Mantle* sample is practically negligible in the case of the MSW SMA solution of interest [19], we have for the D-N asymmetry measured using the night N5 bin data: $A_{D-N}^{N5} \cong 0.8A_{D-N}^C$, A_{D-N}^C being

*Being a constructive interference effect between the amplitudes of neutrino transitions in the mantle and in the core, this is not just “core enhancement” effect, but rather *mantle-core enhancement* effect.

†The term “neutrino oscillation length resonance” (NOLR) was used in [23], in particular, to denote the mantle-core enhancement effect in this case.

the asymmetry in the *Core* sample. The data on A_{D-N}^{N5} [5] permitted to exclude a part of the MSW SMA solution region located in the area $\sin^2 2\theta_V \cong (0.007 - 0.01)$, $\Delta m^2 \cong (0.5 - 1.0) \times 10^{-5} \text{ eV}^2$. Let us note that it was possible to probe the indicated MSW SMA solution region only due to the *mantle-core enhancement* [23–25] of the the *Core* part of the asymmetry A_{D-N}^{N5} . It should be obvious from the above discussion that the measurement of the *Core* asymmetry A_{D-N}^C , as suggested in [19], will provide a more effective test of the the MSW SMA solution [‡] than the measurement of A_{D-N}^{N5} .

As was shown in [20,23], the *mantle-core enhancement* is not so effective in the ^8B neutrino energy interval $E \sim (5 - 12) \text{ MeV}$ when the solar neutrino transitions are of the type $\nu_e \rightarrow \nu_s$: it does not produce such a dramatic enhancement of the *Core* D-N asymmetry as in the case of $\nu_e \rightarrow \nu_{\mu(\tau)}$ transitions. More generally, the measurements of the D-N effect related observables in the Super-Kamiokande experiment appears at present unlikely to provide an effective test of the MSW $\nu_e \rightarrow \nu_s$ (SMA) solution of the solar neutrino problem [20].

The studies of the D-N effect will be continued by the SNO experiment which is already operational [27]. As is well known, the solar neutrinos can be detected in SNO via the charged current (CC) reaction on deuterium,

$$\nu_e + D \rightarrow e^- + p + p, \quad (CC) \quad (3)$$

deuterium break up by neutrinos via the neutral current (NC) weak interaction,

$$\nu + D \rightarrow \nu + n + p, \quad (NC) \quad (4)$$

and via the elastic scattering (ES) on electrons,

$$\nu + e^- \rightarrow \nu + e^-. \quad (ES) \quad (5)$$

In the present article we derive detailed predictions for the D-N asymmetries in the CC, NC and ES event rates for the SNO detector. For the ^8B neutrino flux, $\Phi(B)$, which at the Earth surface represents 47.5% of the flux predicted by the standard solar model [8], $\Phi_{SSM}(B)$, the expected number of events per year due to the CC reaction $\nu_e + D \rightarrow e^- + p + p$ in the SNO detector is about [27] 3300 for $T_{e,th} = 5 \text{ MeV}$, $T_{e,th}$ being the threshold kinetic energy of the final state e^- . This is comparable to the event rate in the Super - Kamiokande experiment. The expected event rate [27] due to the NC reaction $\nu_l + D \rightarrow \nu_l + n + p$ for a full standard solar model [8] ^8B neutrino flux (and 45% detection efficiency) is approximately (5.5 - 6.0) events per day, while the event rate due to the $\nu - e^-$ elastic scattering (ES) reaction is predicted to be ~ 1.4 events per day for $\Phi(B) \sim 0.47\Phi_{SSM}(B)$ and $T_{e,th} = 5 \text{ MeV}$. The indicated statistics permits to perform a high precision search for the D-N effect and for the Earth *mantle-core enhancement* of the effect in the sample of events due to the CC reaction. Therefore the main emphasis of our study will be on the predictions for the magnitude of the D-N effect in the CC sample of events in the SNO detector, although rather detailed results for the expected magnitude of the effect in the ES and NC samples will also be presented. Let us remind the reader that the D-N asymmetry in the NC event rate can be nonzero in the case of the MSW solution of the solar neutrino problem with transitions into sterile neutrino [14].

Predictions for the D-N effect for the SNO detector were derived in refs. [13,16,21,22] and recently in [28]. However, our study overlaps little with those performed in [13,16,21,22,28].

[‡]We were happy to learn [26] that recently the Super-Kamiokande collaboration has decided to present experimental results on the *Core* D-N asymmetry as well.

2. Calculating the D-N Effect for the SNO Detector

2.1. The CC and NC Reaction Cross Section Uncertainties

The high precision calculations of the D-N effect for the SNO detector performed in the present article are based on the methods developed for our studies of the D-N effect for the Super-Kamiokande detector, which are described in detail in [18–20]. The cross sections of the CC and NC reactions on deuterium were taken from [29–31]. They were tabulated using the 1996 version of the E. Lisi νd FORTRAN library [32]. The cross section of the $\nu_e - e^-$ elastic scattering reaction was taken from [33]. We used in our calculations the ^8B neutrino spectrum derived in [34]. The probability of survival of the solar ν_e when they travel in the Sun and further to the surface of the Earth, $\bar{P}_\odot(\nu_e \rightarrow \nu_e)$, was computed on the basis of the analytic expression obtained in [35] and using the method developed in [36]. In the calculation of $\bar{P}_\odot(\nu_e \rightarrow \nu_e)$ we have utilized (as in [18–20]) the density profile of the Sun and the ^8B neutrino production distribution in the Sun, predicted in [37]. These predictions were updated in [8], but a detailed test study showed [38] (see also [22]) that using the results of [8] instead of those in [37] leads to a change of the survival probability by less than 1% for any set of values of the parameters Δm^2 and $\sin^2 2\theta$, relevant for the calculation of the D-N effect. As in [18–20], the Earth matter effects were calculated using the Stacey model from 1977 [39] for the Earth density distribution. The latter practically coincides with that predicted by the more recent Earth model [40]. Most of the results are obtained for two sets of values of the electron fraction number in the Earth mantle and the Earth core, $Y_e(\text{man})$ and $Y_e(\text{core}) \equiv Y_e^c$, which reflect the chemical composition of the two major Earth structures: the standard ones $Y_e(\text{man}) = 0.49$, $Y_e^c = 0.467$, and for the possibly conservative upper bound of $Y_e^c = 0.500$ (see, e.g. [41,19]). The latter effectively accounts for the uncertainties both in Y_e^c and in the average matter density of the Earth core.

Three different calculations of the cross section of the $\nu_e - D$ CC reaction are available in the literature [29–31]. In two of these articles [30,31] the cross section of the $\nu_l - D$ NC reaction was also computed. Extensive numerical study has shown that i) the *maximal* differences between the various one year averaged D-N asymmetries in the CC event rate, calculated using the three different predictions for the CC cross section, do not exceed 6%, ii) the differences in the range of (1 - 6)% occur only in a set of disconnected regions in the $\Delta m^2 - \sin^2 2\theta_V$ plane, which are essentially point-like and whose total area is exceedingly small, and iii) these small point-like regions of maximal spread in the D-N asymmetry predictions are generally located outside and sufficiently far from the MSW solution regions of interest (including the “conservative” ones). There is only one case when such a difference occurs on the borderline of an MSW “conservative” solution region: we found a spread in the prediction for D-N asymmetry in the *Core* sample of events of $\sim 2.5\%$ in the case of $\nu_e \rightarrow \nu_{\mu(\tau)}$ transitions for $\sin^2 2\theta \sim 0.6$ and $\Delta m^2 \sim 3 \times 10^{-5} \text{ eV}^2$, which is at the border of the LMA “conservative” solution region.

The cross sections of the $\nu_e - D$ CC reaction calculated in [29–31] differ by $\sim (5 - 15)\%$ at the ^8B neutrino energies of interest. The question of why the predicted D-N asymmetries in the CC and NC event rates are so insensitive to the choice of the cross section used in the calculations naturally arises. The product of the normalized to one ^8B neutrino spectrum, $\mathcal{S}(E)$, and of the CC reaction cross section, $\sigma_{CC}(E)$, which enters into the expression for the CC event rate, can be approximated by a resonance-like function defined by its full width at half maximum, the position of the maximum in E and by its value at the maximum. These parameters were calculated for the three different cross sections [29–31] and for different values of the threshold kinetic energy of the final state electron, $T_{e,th}$. The results are given in Table I. The largest differences between the three results for $\mathcal{S}(E)\sigma_{CC}(E)$ happen in the fastly decreasing part of the ^8B neutrino spectrum ($E \gtrsim 10 \text{ MeV}$). As Table I shows, the spread in the values at the maximum is between 3.5% and 10%, while the position

of the maximum in E and the F.W.H.M. change at most by 0.8%. Consequently, the differences between the three CC cross sections [29–31] lead essentially only to a non-negligible change in the prediction for the overall normalization factor for the total CC event rate, which practically does not affect the D-N asymmetry. The same conclusions can be shown to be valid for the implications of the differences between the two NC cross sections [30,31] for the uncertainties in the predicted values of the D-N asymmetries in the NC signal in SNO in the case of MSW $\nu_e \rightarrow \nu_s$ transition solution of the solar neutrino problem. These results are illustrated in Figs. 1a - 1f, where the difference between the values of the *Core* (*Night*) D-N asymmetry calculated utilizing the predictions for the relevant CC and NC reaction cross-sections derived in ref. [30] and in ref. [31] are shown as functions of Δm^2 and $\sin^2 2\theta_V$ in the intervals $(10^{-7} - 10^{-4})$ eV² and $(10^{-4} - 1.0)$, respectively [§].

This analysis permits one to conclude that even neglecting the electron energy resolution function and the expected statistical and systematic errors in the measurements, the calculation of the D-N asymmetries in the CC and NC event rates in the SNO detector utilizing the different cross sections from [29–31] should give the same results within 1% in the MSW “conservative” solution regions. Accordingly, we will present predictions for the D-N asymmetries in the CC and NC signals computed using the cross sections of ref. [30].

2.2 Comments on the Probability of Solar ν_e Survival

The SNO detector is located at $\lambda_{\text{SNO}} = 46^\circ 20'$ North, $\lambda'_{\text{SNO}} = 81^\circ 12'$ West. At the indicated latitude we have: $T_{res}^C/T_y = 0.0396$, where T_{res}^C is the *Core* residence time, i.e., the total time in one year during which the solar neutrinos cross the Earth core at night on the way to the SNO detector, $T_y = 365.24$ days. This implies that at the location of the SNO experiment only for 7.9% of the one year night time the Sun is behind the Earth core with respect to SNO, to be compared with 14.85% for the Super - Kamiokande detector (see, e.g., [18]). Thus, the statistical error in the measurement of the *Core* D-N asymmetry with SNO detector will be approximately by a factor of 3.55 bigger than in the measurement of the *Night* D-N asymmetry. In the case of the Super - Kamiokande detector this factor is 2.66. Let us note also that for the *Mantle* residence time, T_{res}^M , i.e., the total time in one year during which the solar neutrinos cross at night the Earth mantle but do not cross the Earth core on the way to the SNO detector, we have $T_{res}^M/T_y = 0.4619$, and that the *Night* residence time is $T_{res}^N = 0.5015T_y$.

As is well-known, one can use the $\nu_2 \rightarrow \nu_e$ transition probability, P_{e2} , to account for the Earth matter effects in the solar ν_e survival probability, $\bar{P}(\nu_e \rightarrow \nu_e)$, in the case of the MSW solutions of the solar neutrino problem. During the day one has $\bar{P}(\nu_e \rightarrow \nu_e) = \bar{P}_\odot(\nu_e \rightarrow \nu_e)$, where $\bar{P}_\odot(\nu_e \rightarrow \nu_e)$ was defined earlier as the probability of survival of the solar ν_e when they travel to the Earth surface without traversing the Earth. A nonzero difference between $\bar{P}(\nu_e \rightarrow \nu_e)$ for the Earth-crossing neutrinos and $\bar{P}_\odot(\nu_e \rightarrow \nu_e)$ produces a nonzero D-N asymmetry. It is possible to have $\bar{P}(\nu_e \rightarrow \nu_e) - \bar{P}_\odot(\nu_e \rightarrow \nu_e) \neq 0$ when i) $\bar{P}_\odot(\nu_e \rightarrow \nu_e) \neq 0.5$ and ii) P_{e2} differs from its value in vacuum, $P_{e2} \neq \sin^2 \theta_V$ (for further details see, e.g., [18–22]).

We have calculated the one year averaged $\nu_2 \rightarrow \nu_e$ transition probability for the location of the SNO detector, $\langle P_{e2} \rangle$, using the methods described in [18]. As in [18], this was done for each of the three different event samples *Core*, *Night* and *Mantle* we are considering, $\langle P_{e2} \rangle^{C,N,M}$. We comment below only on few specific features of the probabilities $\langle P_{e2} \rangle^{C,N,M}$ and of the corresponding solar

[§]However, all the plots produced in the framework of this study are at disposition of the interested reader at the site <http://www.pv.infn.it/~maris/nue/sno/index.html>.

ν_e survival probabilities at night, $\bar{P}^{C,N,M}(\nu_e \rightarrow \nu_e)$.

2.2.1 $\nu_e \rightarrow \nu_{\mu(\tau)}$ Transitions

At small mixing angles, $\sin^2 2\theta_V \lesssim 0.01$, $\langle P_{e2} \rangle^C$ is considerably larger than $\langle P_{e2} \rangle^{N,M}$ in most of the interval of values of $E_\nu/\Delta m^2$ of interest: the absolute maximum of $\langle P_{e2} \rangle^C$, for instance, exceeds the absolute maxima of $\langle P_{e2} \rangle^{N,M}$ by a factor of $\sim (4-5)$. This is illustrated in Figs. 2a - 2b. The strong resonance-like enhancement of $\langle P_{e2} \rangle^C$ with respect to $\langle P_{e2} \rangle^{N,M}$, seen, in particular, in Figs. 2a - 2b, is ** due to a constructive interference between the amplitudes of the neutrino transitions in the Earth mantle and in the core [23–25]. The interference produces points of total neutrino conversion [24,25], $\max(P_{e2}) = 1$. For each fixed \hat{h} from the interval $\hat{h} = (0^\circ - 30^\circ)$, there exists one such point in the region $\sin^2 2\theta_V \leq 0.10$, located in the interval $\sin^2 2\theta_V \cong (0.04 - 0.08)$ (see Table 4 in [25]). At $\hat{h} = 23^\circ$, for instance, we have $\max(P_{e2}) = 1$ at $\sin^2 2\theta_V = 0.06$ and $\Delta m^2/E = 6.5 \times 10^{-7}$ eV²/MeV ††. The probability P_{e2} is enhanced at each given $\hat{h} \lesssim 30^\circ$ in a sufficiently wide region in the neighborhood of the corresponding point of total neutrino conversion, which causes the strong enhancement of $\langle P_{e2} \rangle^C$ under discussion at $\sin^2 2\theta_V \lesssim 0.01$.

For $\sin^2 2\theta_V \lesssim 0.004$, $\langle P_{e2} \rangle^{C,N,M}$ are nonnegligible in an interval of values of $E/\Delta m^2$ where $\bar{P}_\odot(\nu_e \rightarrow \nu_e) > 0.5$ and the D-N asymmetries (defined as in eq. (1)) for all the three samples of events *Core*, *Night* and *Mantle*, $A_{D-N}^{C,N,M}$, are negative. For the values of Δm^2 from the SMA solution region and the neutrino energies of interest, $E \cong (5.0 - 14.4)$ MeV, the core asymmetry A_{D-N}^C goes through zero in the interval of $\sin^2 2\theta_V \cong (0.004 - 0.006)$. For each given value of $\sin^2 2\theta_V$ from this interval the zero D-N effect line $\bar{P}_\odot(\nu_e \rightarrow \nu_e) = 0.5$ taking place at a specific value of $E/\Delta m^2$, $(E/\Delta m^2)_0$, splits $\langle P_{e2} \rangle^C$ into two parts: the part at $E/\Delta m^2 > (E/\Delta m^2)_0$ generates a negative D-N asymmetry, while the part at $E/\Delta m^2 < (E/\Delta m^2)_0$ creates a positive D-N asymmetry. When integrating over the neutrino energy the positive and the negative contributions to A_{D-N}^C tend to mutually cancel. For each given $\sin^2 2\theta_V \cong (0.004 - 0.006)$ there exists a Δm^2 from the SMA solution region for which this cancellation is exact giving $A_{D-N}^C = 0$. In the case of the *Night* asymmetry, the interval in $\sin^2 2\theta_V$ in which one has $A_{D-N}^N = 0$ for a certain value of Δm^2 from the SMA solution region is larger: $\sin^2 2\theta_V \cong (0.004 - 0.008)$. For $\sin^2 2\theta_V \gtrsim 0.006$ (0.008) we have $A_{D-N}^C > 0$ ($A_{D-N}^N > 0$).

As in [18], one can introduce the probability D-N asymmetries,

$$A_P^{C,N,M} = \frac{\bar{P}^{C,N,M}(\nu_e \rightarrow \nu_e) - \bar{P}_\odot(\nu_e \rightarrow \nu_e)}{0.5(\bar{P}^{C,N,M}(\nu_e \rightarrow \nu_e) + \bar{P}_\odot(\nu_e \rightarrow \nu_e))}, \quad (6)$$

which give an indication about the possible magnitude of the corresponding energy-integrated event rate asymmetries. For $\sin^2 2\theta_V < 0.004$, $A_P^{C,N}$ are essentially negative and we have $|A_P^C| \lesssim 3.0\%$; 4.7%, while $|A_P^N| \lesssim 1\%$. At $\sin^2 2\theta_V = 0.004$, A_P^C and A_P^N as functions of $E/\Delta m^2$ have substantial positive and negative parts and $-4\% \lesssim A_P^C \lesssim 5.0\%$, $-1.5\% \lesssim A_P^N \lesssim 3.5\%$. As $\sin^2 2\theta_V$ increases beyond the zero asymmetry region, A_P^C increases steadily while the increase of A_P^N is rather slow. At $\sin^2 2\theta_V = 0.008$; 0.010, for instance, A_P^C reaches the values of $\sim 26\%$; 50% and $A_P^N \lesssim 2.7\%$; 8.0%. This corresponds to an enhancement factors of the *Core* asymmetry at the maxima of ~ 9.6 ; 6.3. The

**The plots of $\langle P_{e2} \rangle^{C,N,M}$ as functions of $\Delta m^2/E$ at fixed $\sin^2 2\theta_V \lesssim 0.01$ are very similar to those for the Super-Kamiokande detector, published in ref. [18] which includes a large set of such plots.

†† The points under discussion change somewhat their position with the change of \hat{h} (see Table 4 in [25]).

above results suggests that for values of $\sin^2 2\theta_V$ from the SMA solution region, the *Core* event rate asymmetry in SNO can be bigger than the *Night* asymmetry by factors which can exceed the similar factors for the predicted *Core* and *Night* asymmetries in the Super-Kamiokande detector: in the latter case the *Core* asymmetry enhancement factor does not exceed ~ 6 [18,19].

It is interesting to note that for $\sin^2 2\theta_V \cong (4 - 10) \times 10^{-3}$, $A_P^{C,N}$ have relatively large positive values at $E/\Delta m^2 \approx \text{few} \times 10^{-5} \text{ MeV/eV}^2$. In the same region $A_P^{C,N}$ exhibit (as functions of $E/\Delta m^2$) fast small amplitude oscillations as well. These maxima of $A_P^{C,N}$ are responsible for the noticeable “horn” at $\sin^2 2\theta_V \gtrsim 5 \times 10^{-3}$ and $\Delta m^2 \gtrsim 2 \times 10^{-5} \text{ eV}^2$, shown by the CC and NC D-N asymmetry contour plots in the case of the $\nu_e \rightarrow \nu_{\mu(\tau)}$ and $\nu_e \rightarrow \nu_s$ transitions, as well as by the ES D-N asymmetry contour plots for $\nu_e \rightarrow \nu_s$ transitions (see further). The lack of a similar “horn” in the ES D-N asymmetry contour plots in the $\nu_e \rightarrow \nu_{\mu(\tau)}$ case is due to the neutral current contribution of $\nu_{\mu(\tau)}$ to the ES event rate. The indicated feature of $A_P^{C,N}$ affects the D-N asymmetries of interest only for a set of neutrino parameters which lie outside the regions of the MSW solutions and we are not going to discuss it further.

The *mantle-core enhancement* of A_P^C [23–25] is much less dramatic in the region of the LMA solution: actually, in this region we typically have $A_P^C \cong (1.0 - 1.25)A_P^N$, with A_P^C exhibiting as a function of $E/\Delta m^2$ rather large amplitude oscillations which are absent in A_P^N .

2.2.2 $\nu_e \rightarrow \nu_s$ Transitions

The Earth *mantle-core enhancement* of P_{e2} at small mixing angles is operative in the case of $\nu_e \rightarrow \nu_s$ transitions as well [20,23–25]. For $\sin^2 2\theta_V \cong (0.1 - 1.0) \times 10^{-2}$ the corresponding absolute maximum of the one-year averaged *Core* probability $\langle P_{e2} \rangle^C$ exceeds the absolute maximum of $\langle P_{e2} \rangle^N$ by a factor of ~ 4 . However, at $\sin^2 2\theta_V \lesssim 0.01$, $\langle P_{e2} \rangle^C$ is noticeably smaller in the case of $\nu_e \rightarrow \nu_s$ transitions of the solar neutrinos than in the case of the $\nu_e \rightarrow \nu_{\mu(\tau)}$ transitions considered above (for illustration see the corresponding plots for the Super-Kamiokande detector in [20]). For $\sin^2 2\theta_V = 0.01$, for instance, the maximal values reached by $\langle P_{e2} \rangle^C$ in the two cases are ~ 0.1 and ~ 0.3 , respectively. Similar result was shown [20] to be valid for $\langle P_{e2} \rangle^C$ calculated for the location of the Super-Kamiokande detector. The explanation of this difference can be found in [25]: it is related to the fact that the total neutrino conversion point at $\sin^2 2\theta_V \lesssim 0.25$, which determines the enhancement under discussion, takes place for the different \hat{h} at $\sin^2 2\theta_V \cong (0.12 - 0.25)$, which is relatively “far” in $\sin^2 2\theta_V$ from the region of interest (see Table 4 in [25]). The primary source is, of course, the difference between the neutrino effective potentials in matter in the two cases [42] (see also, e.g., [20]).

For $\sin^2 2\theta_V \lesssim (0.009 - 0.010)$, the probability D-N asymmetries for the *Core* and *Night* event samples have (as functions of $E/\Delta m^2$) substantial negative parts in addition to the positive ones. For most of the indicated values of $\sin^2 2\theta_V$ and the values of Δm^2 from the MSW $\nu_e \rightarrow \nu_s$ solution region and of the neutrino energy of interest, $E \geq 6.44 \text{ MeV}$, the energy-integrated D-N asymmetries A^C and A^N are determined essentially by the negative parts of A^C and A^N and therefore are negative. The zero asymmetry regions take place for A^C and A^N roughly at $\sin^2 2\theta_V \sim 0.009$ and $\sin^2 2\theta_V \sim 0.010$, respectively. At small mixing angles, $\sin^2 2\theta_V \lesssim 0.010$, the CC asymmetries are relatively small. For $\sin^2 2\theta_V = (0.003 - 0.010)$, for instance, one finds $-3.0\% \lesssim A_P^C \lesssim 8.0\%$ and $-0.8\% \lesssim A_P^N \lesssim 6.0\%$.

The solar neutrino data strongly disfavors large mixing angle MSW solution in the case of $\nu_e \rightarrow \nu_s$ transitions. Nevertheless, we would like to note that due to the existence of points of absolute minima of the probability P_{e2} for the solar neutrinos crossing the Earth core [25], $\min(P_{e2}) = 0$, one finds at $\sin^2 2\theta \sim (0.4 - 0.5)$ a large negative *Core* probability asymmetry, $\min(A_P^C) \cong -70\%$, at $E/\Delta m^2 \sim (2 - 3) \times 10^6 \text{ MeV/eV}^2$.

2.2.3 On the Latitude Dependence of the Core Asymmetry Enhancement

The comparison of $\langle P_{e2} \rangle^C = \langle P_{e2} \rangle^C(\rho_r)$ plots at fixed $\sin^2 2\theta_V \lesssim 0.01$ for the Super-Kamiokande detector [18,20], where

$$\rho_r \equiv \frac{\Delta m^2 \cos 2\theta_V}{\sqrt{2}G_F E} m_N, \quad (7)$$

m_N being the nucleon mass, with those for the SNO detector shows that the main effect on $\langle P_{2e} \rangle^C$ of a moderated increase of the SNO detector latitude is a shift of the position of the dominating absolute maximum of $\langle P_{2e} \rangle^C$ and not a reduction of this maximum. Thus, the magnitude of the *mantle-core enhancement* for moderate increase of the detector latitude, and therefore the sensitivity of the SNO detector to the D-N effect, is primarily affected by the reduction in the *Core* residence time and by changes in the position of the $\langle P_{e2} \rangle^C$ dominating maximum along the ρ_r axis with respect to the $\bar{P}_\odot(\nu_e \rightarrow \nu_e) = 1/2$ line. This observation suggests that for SNO, ICARUS and other solar neutrino detectors situated at latitudes which are somewhat larger than that of the Super-Kamiokande detector, the sensitivity to the D-N effect may be better than is usually expected.

To understand this result it is helpful to consider the dependence of P_{e2} on ρ_r and the Nadir angle \hat{h} . The behavior of $\langle P_{e2} \rangle^C$ follows from this dependence. At small $\sin^2 2\theta_V$ and for any fixed value of ρ_r (or $E/\Delta m^2$), P_{e2} is a decreasing function of \hat{h} for the Earth-core-crossing neutrinos \ddagger . Since the time averaged \hat{h} for the core-crossing neutrinos increases with the increasing of the detector latitude and given the fact that SNO is at a higher latitude than the Super-Kamiokande detector, a smaller $\langle P_{e2} \rangle^C$ probability is expected for SNO than for the Super-Kamiokande detector, which seems to be in contradiction with the suggestion made above. A more detailed study of the ρ_r and \hat{h} dependence of P_{e2} at fixed $\sin^2 2\theta_V \lesssim 0.01$ reveals, however, that in the region of the absolute maximum of P_{2e} (at a given $\sin^2 2\theta_V$) this dependence can be described as a part of a *positive saddle* with fastly decreasing “shoulders”, but whose main axis (i.e., the “ridge” or minimal gradient line) is curved towards smaller values of ρ_r when \hat{h} increases (Fig. 3). Moreover, along its main axis and on a relatively large part of it, the *saddle* is nearly flat and therefore P_{2e} changes very little. The plots of P_{2e} versus \hat{h} at fixed ρ_r are sections of the *saddle* at high inclination with respect of the *saddle axis*, so what they illustrate is the fast decrease of the saddle shoulders. The plots of the P_{2e} dependence on ρ_r at fixed but different \hat{h} show the shift of the position of the maximum along the ρ_r -axis for changing \hat{h} , thus exhibiting the curvature of the saddle axis. The behavior of P_{2e} discussed above is illustrated in Fig. 3.

When translating these considerations into total event rate predictions, one obviously has to take into account the effects of the shape of the 8B neutrino spectrum and of the integration over the neutrino energy. For $\sin^2 2\theta_V$ in the range of $\sim (10^{-3} - 10^{-2})$, the D-N effect is suppressed by the simultaneous presence of a negative and positive parts of the D-N probability asymmetry in the interval of values of $E/\Delta m^2$ of interest [18]. As already discussed above, one of the important parameters which determine for given $\sin^2 2\theta_V$ the magnitude of the D-N effect is the position of the absolute maximum of $\langle P_{2e} \rangle^C$ along the $E/\Delta m^2$ axis with respect to the zero asymmetry

\ddagger This is related to the fact that with the increase of \hat{h} the position of the total neutrino conversion point where $P_{e2} = 1$, which determines the magnitude of the mantle-core enhancement of P_{e2} at $\sin^2 2\theta_V \lesssim 0.01$, shifts to larger values of $\sin^2 2\theta$ [25], e.g., from $\sin^2 2\theta \cong 0.04$ at $\hat{h} = 13^\circ$ to $\sin^2 2\theta \cong 0.08$ at $\hat{h} = 30^\circ$ in the $\nu_e \rightarrow \nu_{\mu(\tau)}$ case. The indicated shift is caused, in particular, by the decreasing of the neutrino path length through the Earth core and of the average density of the core along the neutrino path when \hat{h} increases.

line $E/\Delta m^2 = (E/\Delta m^2)_0$ corresponding to $\bar{P}_\odot = 1/2$. The shift towards smaller values of ρ_r (or larger values of $E/\Delta m^2$) of the position of the dominating maximum of $\langle P_{2e} \rangle^C$ as the detector latitude increases makes the crossing of the $\bar{P}_\odot = 1/2$ line by the maximum occur at larger values of $\sin^2 2\theta_V$. Thus, for a given $\sin^2 2\theta_V \lesssim 0.009$, the region of negative values of A_P^C in $E/\Delta m^2$ increases somewhat with the increase of \hat{h} at the expense of the region where $A_P^C > 0$. This results in a certain decreasing of the CC total event rate *Core* D-N asymmetry A_{D-N}^C . Similar effect takes place for the *Night* asymmetry A_{D-N}^N . The decreasing is roughly the same in magnitude as the one caused by the presence of the NC contribution due to the $\nu_{\mu(\tau)}$ in the Super-Kamiokande solar neutrino signal in the case of the MSW $\nu_e \rightarrow \nu_{\mu(\tau)}$ transitions of solar neutrinos. Actually, the ratio A_{D-N}^C/A_{D-N}^N of the discussed asymmetries for SNO is typically bigger, as we shall see, than that for the Super-Kamiokande detector. This analysis shows also that in the case of the MSW SMA $\nu_e \rightarrow \nu_{\mu(\tau)}$ solution the enhancement of the *Core* D-N asymmetry in the CC event rates for detectors located at different latitudes not exceeding, say, the SNO latitude ($\lambda_{\text{SNO}} = 46^\circ 20'$ North), is approximately the same in magnitude and that the sensitivity to the *Core* D-N effect, apart from the systematic error, is limited essentially by the statistics of the corresponding data samples.

3. Predictions for the Energy-Integrated D-N Asymmetries

In this Section we will discuss the predictions we have obtained for the values of the various energy-integrated, one year averaged D-N asymmetries for the SNO detector. The asymmetries are defined as in eq. (2) and in [18–20]. We consider the following set of D-N asymmetries: i) *Night*, *Core* and *Mantle* asymmetries in the CC signal in SNO, $A_{D-N}^{N,C,M}(CC) = A_{D-N}^{N,C,M}(CC; T_{e,th}, Y_e^c)$, in the case of the $\nu_e \rightarrow \nu_{\mu(\tau)}$ and $\nu_e \rightarrow \nu_s$ transitions of solar neutrinos, ii) *Night*, *Core* and *Mantle* asymmetries in the ES signal in SNO, $A_{D-N}^{N,C,M}(ES) = A_{D-N}^{N,C,M}(ES; T_{e,th}, Y_e^c)$, in the case of the $\nu_e \rightarrow \nu_{\mu(\tau)}$ and $\nu_e \rightarrow \nu_s$ transitions, and iii) *Night*, *Core* and *Mantle* asymmetries in the NC signal in SNO, $A_{D-N}^{N,C,M}(NC) = A_{D-N}^{N,C,M}(NC; Y_e^c)$, in the case of the $\nu_e \rightarrow \nu_s$ transitions^{§§}. The asymmetries $A_{D-N}^{N,C,M}(CC; T_{e,th}, Y_e^c)$ and $A_{D-N}^{N,C,M}(ES; T_{e,th}, Y_e^c)$ have been calculated for two values of $T_{e,th}$: 5.0 MeV and 7.5 MeV. Results for all asymmetries for $Y_e(\text{core}) = 0.467$ and 0.500 [19] are given^{***}.

Our results are presented in Tables II - X and in Figs. 4a - 11b. The tables contain values of the three types of asymmetries and of the ratio of the *Core* and *Night* asymmetries, calculated for 36 pairs of values of Δm^2 and $\sin^2 2\theta_V$ distributed evenly in the “conservative” MSW solution regions (older and most recent). Some of these pairs of values, as like those with $\sin^2 2\theta_V \gtrsim 0.03$ in the case of MSW $\nu_e \rightarrow \nu_s$ solution in Tables VI - X, have been excluded by the recent Super-Kamiokande data, but we kept them for giving an idea about the magnitude of the asymmetries corresponding to them. In Figs. 4a - 11b contours of constant (D-N) asymmetries in the $\Delta m^2 - \sin^2 2\theta_V$ plane are shown (iso-(D-N) asymmetry contour plots) together with the “conservative” MSW solution regions from [11]. We did not include in the present work the iso-(D-N) asymmetry contour plots for the different (CC, ES, NC) *Mantle* asymmetries because the latter are relatively small and thus difficult

^{§§}Note that with the definition of the D-N asymmetry we use [18–20], the one year average energy-integrated D-N asymmetries we consider are zero in the case of massless standard model neutrinos.

^{***}Predictions for the *Night* CC asymmetry $A_{D-N}^N(CC; T_{e,th}, Y_e^c)$ for $T_{e,th} = 5$ and $T_{e,th} = 5.0; 7.5$ MeV for the standard values of $Y_e(\text{man})$ and $Y_e(\text{core})$ were given respectively in [21,22] and [28]. Results for the *Night* asymmetry in the NC data $A_{D-N}^N(NC)$ for the standard values of $Y_e(\text{man})$ and $Y_e(\text{core})$ were obtained also in [28].

to observe ^{†††}. Below we comment briefly our results for the indicated D-N asymmetries.

3.1. Magnitude of the Asymmetries and their $Y_e(\text{core})$ and $T_{e,th}$ Dependence

3.1.1. $\nu_e \rightarrow \nu_{\mu(\tau)}$ Transitions

A. Asymmetries in the CC Event Sample

The most remarkable feature of the D-N asymmetries under discussion in this case is the relatively large absolute values of the *Core* CC asymmetry $A_{D-N}^C(CC)$ in most of the region MSW SMA solution, as well as the strong *mantle-core enhancement* of $A_{D-N}^C(CC)$ with respect to the *Night* and *Mantle* asymmetries in this region (Tables II and III). Due to the indicated enhancement we typically have $|A_{D-N}^C(CC)| > 1\%$ at $\sin^2 2\theta_V \cong (0.001 - 0.006)$ and $\Delta m^2 \sim (3.0 - 8.0) \times 10^{-6} \text{ eV}^2$, while the *Night* and *Mantle* asymmetries $|A_{D-N}^{N,M}(CC)| < 1\%$ and are hardly observable. The asymmetry $A_{D-N}^C(CC)$ is negative and greater than 1% in absolute value for $\sin^2 2\theta_V \cong (0.7 - 4.0) \times 10^{-3}$ and Δm^2 in the interval above, reaching the minimal value of $\sim (-3.2)\%$ at $\sin^2 2\theta_V \sim 0.002$. The ratio $|A_{D-N}^C(CC)/A_{D-N}^N(CC)|$ varies with $\sin^2 2\theta_V$ and Δm^2 in the MSW SMA solution region typically in the interval of $\sim (5 - 8)$. For $\sin^2 2\theta_V \cong (0.008 - 0.010)$, we have $A_{D-N}^C(CC) \cong (12.9 - 39.7)\%$, while $A_{D-N}^N(CC) \cong (1.8 - 6.6)\%$, the ration between the two asymmetries varying in the range of $\sim (4.3 - 7.9)$. Actually, the CC *Night* asymmetry $A_{D-N}^N(CC)$ is hardly observable at $\sin^2 2\theta_V < 0.008$. The same conclusion is valid for the *Mantle* asymmetry $A_{D-N}^M(CC)$ at $\sin^2 2\theta_V < 0.010$.

The *mantle-core enhancement* of the CC *Core* asymmetry is rather modest in the region of the MSW LMA solution, where we typically have $A_{D-N}^N(CC)/A_{D-N}^N(CC) \sim (1.0 - 1.3)$. Nevertheless, both asymmetries $A_{D-N}^C(CC)$ and $A_{D-N}^N(CC)$ have values exceeding 1% in most of the solution's region (Tables II and III). More specifically, for $\Delta m^2 \lesssim 9.0 \times 10^{-5} \text{ eV}^2$, we have $A_{D-N}^N(CC; 7.5 \text{ MeV}) \gtrsim 2.5\%$ and $A_{D-N}^C(CC; 5.0 \text{ MeV}) \gtrsim 5.0\%$. These predictions suggest that the SNO experiment will be able to probe most of the LMA solution region by measuring the *Night* and/or *Core* D-N asymmetries in the CC event sample. The conclusion is robust against the change of $Y_e(\text{core})$ in the interval 0.467 - 0.500.

Changing $Y_e(\text{core})$ from 0.467 to 0.500 affects little the *Night* CC asymmetry, but can change noticeably, typically by $\sim (10 - 30)\%$, the *Core* asymmetry in the SMA solution region (see, e.g., cases 13 - 19 in Table II and 12-14 and 16 in Table III). For $\sin^2 2\theta_V \sim (0.004 - 0.010)$ and $\Delta m^2 \sim (6.5 - 10.0) \times 10^{-6} \text{ eV}^2$, the change of $A_{D-N}^C(CC)$ can be quite dramatic - the asymmetry increases approximately by a factor of ~ 1.5 . Thus, for values of $\sin^2 2\theta_V$ and Δm^2 from a specific subregion of the MSW SMA solution region the magnitude of the predicted *Core* asymmetry $A_{D-N}^C(CC)$ is very sensitive to the value of the electron fraction number $Y_e(\text{core})$ and the average matter density of the Earth core. The former is determined by the chemical composition of the core [41] (see also [19]). If the MSW SMA solution turned out to be the solution of the solar neutrino problem and the parameters $\sin^2 2\theta$ and Δm^2 lied in the region specified above and are known with a sufficiently high precision, the measurement of the CC *Core* asymmetry can give unique information, e.g., about the chemical composition of the Earth core.

Increasing the value of the threshold kinetic energy of the final state electron $T_{e,th}$ in the CC reaction, eq. (3), from 5.0 MeV to 7.5 MeV can have a dramatic effect on the *Core* asymmetry $A_{D-N}^C(CC)$ changing it by a factor of ~ 2 (compare cases 11, 18 and 20 in Tables II and III). For the values of $\sin^2 2\theta_V$ and Δm^2 for which the *Night* asymmetry $A_{D-N}^N(CC; 5 \text{ MeV}) > 1\%$, the asymmetry

^{†††}These plots can be found at the site: <http://www.pv.infn.it/~maris/nue/sno/index.html>.

for $T_{e,th} = 7.5$ MeV, $A_{D-N}^N(CC; 7.5 \text{ MeV})$, can be both larger or smaller than $A_{D-N}^N(CC; 5 \text{ MeV})$ by at most $\sim 20\%$. For given $\sin^2 2\theta_V$ and Δm^2 from the MSW solution regions there should exist optimal value of $T_{e,th} \gtrsim 5$ MeV for which $|A_{D-N}^C(CC; T_{e,th})|$ and/or $|A_{D-N}^N(CC; T_{e,th})|$ have maximal values.

All the above properties of the *Night* and *Core* CC asymmetries under discussion are exhibited clearly in the corresponding iso-(D-N) asymmetry contour plots for $A_{D-N}^N(CC)$ and $A_{D-N}^C(CC)$, shown in Figs. 4a-4b and 5a-5b, respectively.

B. ES Event Sample Asymmetries

The D-N asymmetries in the ES sample are typically smaller by a factor of ~ 2 than the asymmetries in the CC sample (compare Tables II, III with IV, V). There are exceptions when $A_{D-N}^{C(N)}(ES)$ is of the order of or even larger than $A_{D-N}^{C(N)}(CC)$ but not by factors which can compensate for the much lower statistics expected in the ES sample of SNO. The *mantle-core enhancement* of the *Core* asymmetry at $\sin^2 2\theta \lesssim 0.01$ is operative in this case as well: one typically has $|A_{D-N}^C(ES)/A_{D-N}^N(ES)| \sim (5 - 8)$ (see Tables IV and V).

The above features of the ES sample asymmetries are exhibited in Figs. 6a - 6b and 7a - 7b, representing the iso-(D-N) asymmetry contour plots for $A_{D-N}^N(ES)$ and $A_{D-N}^C(ES)$, respectively, derived for $Y_e(\text{core}) = 0.467; 0.500$ and for $T_{e,th} = 5$ MeV (a) and $T_{e,th} = 7.5$ MeV (b).

3.1.2. $\nu_e \rightarrow \nu_s$ Transitions

The predicted D-N asymmetries of the same type (*Core*, *Night* or *Mantle*) in the CC, ES and NC event samples do not differ much in magnitude in the case of the MSW $\nu_e \rightarrow \nu_s$ transition solution of the solar neutrino problem (Tables VI - X). Let us remind the reader that the observation of a D-N asymmetry in the NC sample of events would be a proof that solar neutrinos undergo transitions into sterile neutrinos [14]: this asymmetry is zero in the case of the $\nu_e \rightarrow \nu_{\mu(\tau)}$ transitions. The main contribution to the energy-integrated D-N asymmetries in the three event samples comes, as in the case of the Super-Kamiokande detector [20], from the ‘‘high’’ energy tail of the ${}^8\text{B}$ neutrino spectrum. This is related to the fact the relevant neutrino effective potential difference in the Earth matter in the case of the $\nu_e \rightarrow \nu_s$ transitions is approximately by a factor of 2 smaller than in the case of $\nu_e \rightarrow \nu_{\mu(\tau)}$ transitions [42,20]. Only the *Core* asymmetries can exceed 1% in absolute value at $\sin^2 2\theta_V \lesssim 0.01$ in specific limited subregions of the ‘‘conservative’’ MSW solution region. The *Night* asymmetries in the ‘‘conservative’’ solution region are for all samples smaller than 1% for $\sin^2 2\theta_V \lesssim 0.01$. In the subregion where $\sin^2 2\theta_V > 0.01$ both the *Core* and *Night* asymmetries for the three event samples, $A_{D-N}^{C,N}(CC)$, $A_{D-N}^{C,N}(ES)$ and $A_{D-N}^{C,N}(NC)$, are greater than 1%, the *Core* asymmetries being larger than the corresponding *Night* asymmetries by a factor of $\sim (2 - 5)$.

The above features can be seen in the corresponding iso-(D-N) asymmetry contour plots shown in Figs. 8a - 8b (CC *Night* asymmetry), 9a - 9c (CC *Core* asymmetry), 10a - 10b (ES *Night* and *Core* asymmetries) and 11a - 11b (NC *Night* and *Core* asymmetries).

Let us note finally that in the subregion $\Delta m^2 \cong (4.0 - 7.0) \times 10^{-6} \text{ eV}^2$, $\sin^2 2\theta \cong (0.009 - 0.020)$, of the ‘‘conservative’’ solution region, the CC *Core* asymmetry $A_{D-N}^C(CC)$ exhibits a very strong dependence on the value of $Y_e(\text{core})$: the change of $Y_e(\text{core})$ from the value of 0.467 to 0.500 leads to an increase of $A_{D-N}^C(CC)$ by a factor of $\sim (2 - 4)$ (see cases 26 - 33 in Tables VI and VII). This becomes evident also by comparing Figs. 9a and 9b.

4. Conclusions

In the present article we have derived detailed predictions for the day-night (D-N) asymmetry

in the energy-integrated one year signals in the SNO detector in the case of the MSW $\nu_e \rightarrow \nu_{\mu(\tau)}$ and/or $\nu_e \rightarrow \nu_s$ transition solutions of the solar neutrino problem. The asymmetries in the charged current (CC), eq. (3), and $\nu - e^-$ elastic scattering (ES), eq. (4), event rates were calculated for both MSW solutions; in the case of the $\nu_e \rightarrow \nu_s$ transition solution the D-N asymmetry in the neutral current (NC) event rate, eq. (5), was derived as well. The asymmetries were calculated for the three night samples of events which are produced by the solar neutrinos crossing i) the Earth mantle only (*Mantle*), ii) the Earth core (*Core*) and iii) the Earth core and/or the mantle (*Night*) on the way to the SNO detector: $A_{D-N}^{C,N,M}(CC)$, $A_{D-N}^{C,N,M}(ES)$ and $A_{D-N}^{C,N,M}(NC)$.

We have studied the effects of the uncertainties in the values of the cross-sections of the CC and NC neutrino-induced reactions on deuterium by comparing the predictions for the asymmetries $A_{D-N}^{C,N,M}(CC)$ and $A_{D-N}^{C,N,M}(NC)$, obtained using the CC cross-sections from refs. [29–31], and the NC cross-sections from refs. [30,31]. Our analysis showed that even neglecting the electron energy resolution function and the expected errors in the measurements, the calculation of the D-N asymmetries in the CC and NC event samples in the SNO detector utilizing the different cross-sections from [29–31] and [30,31], respectively, should give the same results within 1% in the MSW “conservative” solution regions.

As in the case of the same type of D-N asymmetries for the Super-Kamiokande detector [18–20], at small mixing angles the *Core* asymmetries were shown to be considerably larger than the corresponding *Night* and *Mantle* asymmetries due to the *mantle-core enhancement* effect [23–25]. Due to this enhancement, e.g., the one year average *Core* CC asymmetry in the case of the SMA MSW $\nu_e \rightarrow \nu_{\mu(\tau)}$ solution is bigger than 1% in absolute value, $|A_{D-N}^C(CC)| > 1\%$, in large subregions of the “conservative” solution region which extends in $\sin^2 2\theta_V$ from $\sim 0.7 \times 10^{-3}$ to $\sim 10^{-2}$ (Figs. 5a - 5b). In contrast, in the same solution region we have $|A_{D-N}^{N(M)}(CC)| < 1\%$ for the *Night* (*Mantle*) asymmetry at $\sin^2 2\theta_V < 0.008$ (0.010) (Figs. 4a - 4b). The asymmetry $A_{D-N}^C(CC)$ is negative and greater than 1% in absolute value for $\sin^2 2\theta_V \cong (0.7 - 4.0) \times 10^{-3}$ and $\Delta m^2 \sim (3.0 - 8.0) \times 10^{-6} \text{ eV}^2$, reaching the minimal value of $\sim (-3.2)\%$. The ratio $|A_{D-N}^C(CC)/A_{D-N}^N(CC)|$ varies with $\sin^2 2\theta_V$ and Δm^2 in the MSW SMA solution region typically in the interval of $\sim (5 - 8)$ (Tables II and III). For $\sin^2 2\theta_V \cong (0.008 - 0.010)$, we have in this region $A_{D-N}^C(CC) \cong (12.9 - 39.7)\%$, while $A_{D-N}^N(CC) \cong (1.8 - 6.6)\%$.

In the region of the MSW LMA $\nu_e \rightarrow \nu_{\mu(\tau)}$ solution we typically have $A_{D-N}^N(CC)/A_{D-N}^C(CC) \sim (1.0 - 1.3)$. Both asymmetries $A_{D-N}^C(CC)$ and $A_{D-N}^N(CC)$ have values exceeding 1% in most of the solution region (Tables II, III and Figs. 4a - 5b).

The D-N asymmetries in the ES sample in the case of the MSW $\nu_e \rightarrow \nu_{\mu(\tau)}$ solution are in most of the “conservative” solution regions smaller by a factor of ~ 2 than the asymmetries in the CC sample (Tables II, III and IV, V, Figs. 6a - 7b). There are exceptions when $A_{D-N}^{C(N)}(ES)/A_{D-N}^{C(N)}(CC) \gtrsim 1$, but the ratio factors involved cannot compensate for the much lower statistics expected in the ES sample of SNO.

The predicted D-N asymmetries of the same type (*Core*, *Night* or *Mantle*) in the CC, ES and NC event samples do not differ much in magnitude in the case of the MSW $\nu_e \rightarrow \nu_s$ transition solution of the solar neutrino problem (Tables VI - X, Figs. 8a - 11b). Only the *Core* asymmetries can exceed 1% in absolute value at $\sin^2 2\theta_V \lesssim 0.01$ in specific limited subregions of the “conservative” solution region. In the subregion where $\sin^2 2\theta_V > 0.01$ both the *Core* and *Night* asymmetries for the three event samples, are greater than 1%, the *Core* asymmetries exceeding the corresponding *Night* asymmetries by a factor of $\sim (2 - 5)$.

We have found also that in certain subregions of the MSW solution regions at small $\sin^2 2\theta_V$, the predicted magnitude of the *Core* D-N asymmetry in the CC and ES samples is very sensitive to the value of the electron fraction number Y_e^c (i.e., to the chemical composition) and to the average

matter density of the Earth core: the asymmetry $A_{D-N}^C(CC)$, for instance, can increase in the case of the $\nu_e \rightarrow \nu_{\mu(\tau)}$ ($\nu_e \rightarrow \nu_s$) solution by a factor of ~ 1.5 ($2 - 4$) when Y_e^c is changed from the standard value of 0.467 [39,40] to its possibly conservative upper limit of 0.500 [41,19] (Tables II, III, VI, VII, Figs. 5a, 5b, 7a, 7b, 9a-9b).

We have studied the dependence of the D-N asymmetries considered on the final state e^- threshold energy $T_{e,th}$ in the CC and ES reactions. Increasing the value of $T_{e,th}$ in the CC and ES reactions from 5.0 MeV to 7.5 MeV can have a dramatic effect on the *Core* asymmetries $A_{D-N}^C(CC)$ and $A_{D-N}^C(ES)$, changing, e.g., $A_{D-N}^C(CC)$ by a factor of ~ 2 in the case of the $\nu_e \rightarrow \nu_{\mu(\tau)}$ solution (Tables II, III, VI, VII, Figs. 5a, 5b, 9a - 9c).

Our analysis showed also that for the MSW SMA $\nu_e \rightarrow \nu_{\mu(\tau)}$ and $\nu_e \rightarrow \nu_s$ solutions, the enhancement of the *Core* D-N asymmetry in the CC event rates for detectors located at different latitudes not exceeding, say, the SNO latitude ($\lambda_{\text{SNO}} = 46^\circ 20'$ North), is approximately the same in magnitude. This result suggests that for SNO, ICARUS and other solar neutrino detectors operating at latitudes which are somewhat larger than that of the Super-Kamiokande detector, the sensitivity to the *Core* D-N effect, apart from the systematic error, is limited essentially by the statistics of the corresponding data samples.

The results of the present study allow us to conclude, in particular, that the SNO experiment has the potential of probing substantial parts of the SMA and LMA MSW $\nu_e \rightarrow \nu_{\mu(\tau)}$ solution regions by performing *Night* and *Core* D-N asymmetry measurements in the CC event sample. The measurements of the D-N effect related observables with the SNO detector appears unlikely to provide by itself a critical test of the MSW $\nu_e \rightarrow \nu_s$ (SMA) solution of the solar neutrino problem. It is expected that such a test will be provided by the comparison of the CC and NC SNO data. Nevertheless, certain subregions of the “conservative” MSW $\nu_e \rightarrow \nu_s$ solution region can also be probed through the measurements of the D-N effect, e.g., in the CC and NC event samples.

Acknowledgements.

We would like to thank H. Robertson for clarifying discussions concerning the SNO experiment. The work of (S.T.P.) was supported in part by the EC grant ERBFMRX CT96 0090.

REFERENCES

- [1] B. T. Cleveland et al. (Homestake Collaboration), *Astrophys. J.* **496**, 505 (1998).
- [2] Y. Fukuda et al. (Kamiokande Collaboration), *Phys. Rev. Lett.* **77**, 1683 (1996).
- [3] J. N. Abdurashitov et al. (SAGE Collaboration), *Phys. Rev. C* **60**, 055801 (1999).
- [4] W. Hampel et al. (GALLEX Collaboration), *Phys. Lett.* **B447**, 127 (1999).
- [5] Y. Totsuka, in *PANIC'99*, XVth Particle And Nuclei International Conference, June 10 - 17, 1999, Uppsala, Sweden, to be published (available at <http://www-sk.icrr.u-tokyo.ac.jp/doc/pub/>); M. Nakahata, in *TAUP'99*, VIth International Workshop on Topics in Astroparticle and Underground Physics, September 6 - 10, 1999, Paris, France, to appear (transparencies available at <http://taup99.in2p3.fr/TAUP99/>); Y. Fukuda et al., Super-Kamiokande Coll., *Phys. Rev. Lett.* **82** (1999) 1810.
- [6] J. Christensen-Dalsgaard, *Nucl. Phys. B (Proc. Suppl.)* **48**, 325 (1996); J.N. Bahcall et al., *Phys. Rev. Lett.* **78**, 4286 (1997); S. Degl'Innocenti et al., *Astr. Phys.* **7**, 77 (1997).
- [7] J.N. Bahcall, *Neutrino Astrophysics*, Cambridge University Press, Cambridge, 1989.
- [8] J.N. Bahcall, S. Basu and M. Pinsonneault, *Phys. Lett.* **B433**, 1 (1998).
- [9] G.L. Fogli et al., e-Print archive hep-ph/9910387.
- [10] C. Gonzalez-Garcia et al., e-Print archive hep-ph/9906469.
- [11] P.I. Krastev,
Talk given at the *Neutrino Summer '99* Workshop, June - July 1999, TH Division, CERN, Geneva, Switzerland (transparencies available at <http://lyoprs.in2p3.fr/nufact99/talks/>).
- [12] P.I. Krastev and S.T. Petcov, *Phys. Lett.* **B299**, 99 (1993).
- [13] N. Hata and P. Langacker, *Phys. Rev.* **D50**, 632 (1994).
- [14] P.I. Krastev, Q.Y. Liu and S.T. Petcov, *Phys. Rev.* **D54**, 7057 (1996).
- [15] J.N. Bahcall and P.I. Krastev, *Phys. Lett.* **B436**, 243 (1998).
- [16] A.J. Baltz and J. Weneser, *Phys. Rev.* **DD50** (1994) 5971.
- [17] J.M. Gelb, W. Kwong and S.P. Rosen, *Phys. Rev. Lett.* **78** (1997) 2296.
- [18] Q.Y. Liu, M. Maris and S.T. Petcov, *Phys. Rev. D* **56**, 5991 (1997).
- [19] M. Maris and S.T. Petcov, *Phys. Rev. D* **56**, 7444 (1997).
- [20] M. Maris and S.T. Petcov, *Phys. Rev. D* **58**, 113008 (1998).
- [21] E. Lisi and D. Montanino, *Phys. Rev. D* **56**, 3081 (1997).
- [22] J.N. Bahcall and P.I. Krastev, *Phys. Rev. C* **56**, 2839 (1997).
- [23] S.T. Petcov, *Phys. Lett.* **B434**, 321 (1998), (E) **B444**, 584 (1998).
- [24] M. Chizhov and S.T. Petcov, *Phys. Rev. Lett.* **83**, 1096 (1999) (hep-ph/9903399).
- [25] M. Chizhov and S.T. Petcov, hep-ph/9903424.
- [26] We thank Y. Suzuki for communicating to us this decision of the Super-Kamiokande collaboration.
- [27] C.J. Virtue, in *TAUP'99*, VIth International Workshop on Topics in Astroparticle and Underground Physics, September 6 - 10, 1999, Paris, France, to appear (transparencies available at <http://taup99.in2p3.fr/TAUP99/>); see also: e-print archive hep-ex/9910016 and the SNO homepage: <http://ewiserver.npl.washington.edu/sno>.
- [28] J.N. Bahcall, P.I. Krastev and A.Yu. Smirnov, e-Print archive hep-ph/0002293.
- [29] S.D. Ellis, J.N. Bahcall, *Nucl. Phys.* **A114**, 636 (1968).
- [30] K. Kubodera, S. Nozawa, *Int. J. Mod. Phys.* **E3**, 101 (1994).
- [31] S. Ying, W.C. Haxton, E.M. Henley, *Phys. Rev. C* **45**, 1982 (1992).
- [32] J. N. Bahcall, E. Lisi, *Phys. Rev. D.* **54**, 5417 (1996), FORTRAN code from <http://www.sns.ias.edu/~jnb/SNdata/deuteriumcross.html>
- [33] J.N. Bahcall, M. Kamionkowski and A. Sirlin, *Phys. Rev. D* **51**, 6146 (1995).

- [34] J.N. Bahcall et al., Phys. Rev. D **54**, 411 (1996).
- [35] S.T. Petcov, Phys. Lett. **200B**, 373 (1988).
- [36] P.I. Krastev and S.T. Petcov, Phys. Lett. **207B**, 64 (1988).
- [37] J.N. Bahcall, M.H. Pinsonneault, Rev. Mod. Phys. **67**, 781 (1995).
- [38] M. Maris, study performed in 1999, unpublished.
- [39] F.D. Stacey, *Physics of the Earth, 2nd edition*, John Willey and Sons, London, New York, 1977.
- [40] A.D. Dziewonski and D.L. Anderson, Physics of the Earth and Planetary Interiors **25**, 297 (1981).
- [41] R. Jeanloz, Annu. Rev. Earth Planet. Sci. **18**, 356 (1990); C.J. Allègre et al., Earth and Planetary Science Letters **134**, 515 (1995).
- [42] P. Langacker et al., Nucl. Phys. B**282**, 589 (1987).

TABLES

TABLE I. The predicted position of the maximum, value at the maximum and F.W.H.M. of the function $\mathcal{S}(E)\sigma(E)$ for the different reactions used for the detection of the solar neutrinos at SNO. The maximal value for the CC reaction is normalized to the predicted one in ref. [27] for $T_{e,th} = 0$ MeV, while the maximal value for ES reaction is normalized to $T_{e,th} = 0$ MeV.

Reaction	Ref.	$T_{e,th}$ (MeV)	E^{\max} (MeV)	Normalized Maximum Value	F.W.H.M. (MeV)
CC	[29]	0.0	9.58	1.00	5.770
CC	[29]	5.0	9.84	0.94	4.744
CC	[29]	7.5	10.86	0.68	3.049
CC	[30]	0.0	9.60	1.10	5.757
CC	[30]	5.0	9.86	1.04	4.750
CC	[30]	7.5	10.88	0.75	3.076
CC	[31]	0.0	9.58	1.04	5.767
CC	[31]	5.0	9.86	0.98	4.758
CC	[31]	7.5	10.86	0.71	3.055
ES	[33]	0.0	8.04	1.00	6.948
ES	[33]	5.0	9.34	0.40	5.285
ES	[33]	7.5	10.40	0.18	3.932

TABLE II. D - N Asymmetries for the SNO Detector for $T_{e,th} = 5$ MeV, CC, $\nu_e \rightarrow \nu_{\mu(\tau)}$ transition

N.	$\sin^2 2\theta_V$	Δm^2 [eV ²]	$Y_e(\text{core}) = 0.467$				$Y_e(\text{core}) = 0.5$			
			$A_{D-N}^s \times 100$			$\left \frac{A_{D-N}^C}{A_{D-N}^N} \right $	$A_{D-N}^s \times 100$			$\left \frac{A_{D-N}^C}{A_{D-N}^N} \right $
			<i>Night</i>	<i>Core</i>	<i>Mantle</i>		<i>Night</i>	<i>Core</i>	<i>Mantle</i>	
1	0.0008	9×10^{-6}	-0.07	-0.42	-0.03	5.99	-0.08	-0.61	-0.03	7.63
2	0.0008	7×10^{-6}	-0.14	-1.22	-0.05	8.71	-0.15	-1.37	-0.05	9.03
3	0.0008	5×10^{-6}	-0.34	-1.64	-0.29	4.77	-0.34	-1.47	-0.29	4.32
4	0.0010	9×10^{-5}	0.01	0.02	0.01	1.31	0.02	0.02	0.01	1.24
5	0.0010	7×10^{-6}	-0.17	-1.46	-0.06	8.70	-0.18	-1.64	-0.06	9.03
6	0.0010	5×10^{-6}	-0.37	-2.00	-0.30	5.38	-0.37	-1.73	-0.30	4.74
7	0.0020	1×10^{-5}	-0.04	-0.34	-0.02	8.02	-0.06	-0.50	-0.02	9.11
8	0.0020	7×10^{-6}	-0.26	-2.24	-0.11	8.58	-0.29	-2.47	-0.11	8.43
9	0.0020	5×10^{-6}	-0.75	-3.21	-0.56	4.29	-0.72	-2.51	-0.56	3.46
10	0.0040	1×10^{-5}	0.11	0.81	0.05	7.37	0.14	1.23	0.05	8.57
11	0.0040	7×10^{-6}	-0.10	-0.80	-0.05	7.59	-0.10	-0.67	-0.05	7.06
12	0.0040	5×10^{-6}	-0.79	-2.68	-0.63	3.42	-0.75	-2.25	-0.63	2.99
13	0.0060	1×10^{-5}	0.68	4.78	0.28	7.07	0.87	7.06	0.28	8.15
14	0.0060	7×10^{-6}	0.70	6.03	0.24	8.57	0.81	7.28	0.24	8.99
15	0.0060	5×10^{-6}	0.21	2.49	0.01	11.79	0.21	2.53	0.01	11.81
16	0.0080	1×10^{-5}	1.84	13.24	0.81	7.19	2.38	19.12	0.81	8.04
17	0.0080	7×10^{-6}	2.49	19.51	0.87	7.85	2.78	22.59	0.87	8.12
18	0.0080	5×10^{-6}	2.59	12.90	1.65	4.98	2.52	12.06	1.65	4.79
19	0.0100	7×10^{-6}	5.65	39.68	2.05	7.02	6.27	44.77	2.05	7.15
20	0.0100	5×10^{-6}	6.60	28.21	4.45	4.28	6.39	26.10	4.45	4.08
21	0.0130	5×10^{-6}	16.52	57.71	11.86	3.49	16.04	53.77	11.86	3.35
22	0.3000	1.5×10^{-5}	31.49	41.13	30.28	1.31	32.02	46.62	30.28	1.46
23	0.3000	2×10^{-5}	22.22	27.40	21.73	1.23	22.49	30.71	21.73	1.37
24	0.3000	3×10^{-5}	14.04	18.08	13.73	1.29	14.15	19.67	13.73	1.39
25	0.3000	4×10^{-5}	9.59	11.88	9.42	1.24	9.61	12.17	9.42	1.27
26	0.4800	3×10^{-5}	12.98	15.08	12.76	1.16	13.03	15.60	12.76	1.20
27	0.4800	5×10^{-5}	6.39	7.21	6.32	1.13	6.41	7.55	6.32	1.18
28	0.5000	2×10^{-5}	19.86	22.07	19.68	1.11	19.99	23.40	19.68	1.17
29	0.5600	1×10^{-5}	42.73	53.34	41.80	1.25	43.00	56.18	41.80	1.31
30	0.6000	8×10^{-5}	2.60	3.26	2.59	1.25	2.60	3.14	2.59	1.21
31	0.7000	3×10^{-5}	11.48	12.81	11.22	1.12	11.50	13.03	11.22	1.13
32	0.7000	5×10^{-5}	5.95	7.41	5.89	1.25	5.98	7.16	5.89	1.20
33	0.7700	2×10^{-5}	16.37	16.21	16.42	0.99	16.41	16.64	16.42	1.01
34	0.8000	1.3×10^{-4}	0.93	1.15	0.88	1.25	0.92	1.14	0.88	1.24
35	0.9000	4×10^{-5}	6.95	7.93	6.85	1.14	6.95	8.38	6.85	1.21
36	0.9000	1×10^{-4}	1.80	2.11	1.77	1.17	1.80	2.12	1.77	1.18

TABLE III. D - N Asymmetries for the SNO Detector for $T_{e,th} = 7.5$ MeV, CC, $\nu_e \rightarrow \nu_{\mu(\tau)}$ transition

N.	$\sin^2 2\theta_V$	Δm^2 [eV ²]	$Y_e(\text{core}) = 0.467$				$Y_e(\text{core}) = 0.5$			
			$A_{D-N}^s \times 100$			$\left \frac{A_{D-N}^C}{A_{D-N}^N} \right $	$A_{D-N}^s \times 100$			$\left \frac{A_{D-N}^C}{A_{D-N}^N} \right $
			<i>Night</i>	<i>Core</i>	<i>Mantle</i>		<i>Night</i>	<i>Core</i>	<i>Mantle</i>	
1	0.0008	9×10^{-6}	-0.10	-0.54	-0.04	5.34	-0.11	-0.77	-0.04	6.86
2	0.0008	7×10^{-6}	-0.21	-1.84	-0.07	8.70	-0.22	-1.94	-0.07	8.84
3	0.0008	5×10^{-6}	-0.36	-1.28	-0.32	3.53	-0.36	-1.04	-0.32	2.84
4	0.0010	9×10^{-5}	0.00	0.01	0.00	3.43	0.00	0.02	0.00	5.12
5	0.0010	7×10^{-6}	-0.25	-2.21	-0.09	8.69	-0.26	-2.33	-0.09	8.84
6	0.0010	5×10^{-6}	-0.41	-1.52	-0.36	3.74	-0.41	-1.23	-0.36	3.00
7	0.0020	1×10^{-5}	-0.06	-0.49	-0.02	8.06	-0.08	-0.71	-0.02	9.12
8	0.0020	7×10^{-6}	-0.41	-3.38	-0.16	8.22	-0.41	-3.52	-0.16	8.55
9	0.0020	5×10^{-6}	-0.96	-2.55	-0.77	2.67	-0.87	-2.30	-0.77	2.64
10	0.0040	1×10^{-5}	0.10	0.82	0.04	8.25	0.13	1.16	0.04	9.18
11	0.0040	7×10^{-6}	-0.23	-1.73	-0.10	7.56	-0.22	-1.66	-0.10	7.43
12	0.0040	5×10^{-6}	-1.09	-2.70	-0.95	2.48	-1.04	-2.12	-0.95	2.04
13	0.0060	1×10^{-5}	0.65	5.15	0.25	7.94	0.83	7.29	0.25	8.81
14	0.0060	7×10^{-6}	0.80	6.46	0.24	8.05	0.86	7.42	0.24	8.64
15	0.0060	5×10^{-6}	-0.15	0.18	-0.18	1.22	-0.15	0.16	-0.18	1.06
16	0.0080	1×10^{-5}	1.86	14.09	0.74	7.57	2.37	19.59	0.74	8.27
17	0.0080	7×10^{-6}	2.93	22.89	1.01	7.82	3.08	24.47	1.01	7.94
18	0.0080	5×10^{-6}	2.13	6.55	1.75	3.07	2.03	5.21	1.75	2.57
19	0.0100	7×10^{-6}	6.64	45.48	2.35	6.85	6.95	47.96	2.35	6.90
20	0.0100	5×10^{-6}	6.13	16.55	5.14	2.70	5.82	13.31	5.14	2.29
21	0.0130	5×10^{-6}	15.76	37.64	13.52	2.39	15.13	31.03	13.52	2.05
22	0.3000	1.5×10^{-5}	35.12	43.32	34.37	1.23	35.55	49.21	34.37	1.38
23	0.3000	2×10^{-5}	25.43	33.87	24.66	1.33	25.77	37.61	24.66	1.46
24	0.3000	3×10^{-5}	15.94	19.89	15.70	1.25	16.15	21.85	15.70	1.35
25	0.3000	4×10^{-5}	11.47	13.87	11.29	1.21	11.52	14.00	11.29	1.21
26	0.4800	3×10^{-5}	14.70	16.74	14.52	1.14	14.67	18.22	14.52	1.24
27	0.4800	5×10^{-5}	7.63	9.58	7.49	1.26	7.68	9.56	7.49	1.25
28	0.5000	2×10^{-5}	22.58	25.83	22.34	1.14	22.74	27.75	22.34	1.22
29	0.5600	1×10^{-5}	49.45	69.36	47.45	1.40	49.79	72.61	47.45	1.46
30	0.6000	8×10^{-5}	3.42	3.90	3.35	1.14	3.39	4.17	3.35	1.23
31	0.7000	3×10^{-5}	12.90	14.02	12.76	1.09	12.93	14.12	12.76	1.09
32	0.7000	5×10^{-5}	6.98	8.34	6.86	1.19	6.98	8.38	6.86	1.20
33	0.7700	2×10^{-5}	18.32	17.04	18.43	0.93	18.33	17.37	18.43	0.95
34	0.8000	1.3×10^{-4}	1.37	1.57	1.32	1.15	1.35	1.59	1.32	1.18
35	0.9000	4×10^{-5}	8.07	9.24	8.00	1.15	8.10	9.23	8.00	1.14
36	0.9000	1×10^{-4}	2.24	2.53	2.21	1.13	2.24	2.54	2.21	1.14

TABLE IV. D - N Asymmetries for the SNO Detector for $T_{e,th} = 5$ MeV, ES, $\nu_e \rightarrow \nu_{\mu(\tau)}$ transition

N.	$\sin^2 2\theta_V$	Δm^2 [eV ²]	$Y_e(\text{core}) = 0.467$				$Y_e(\text{core}) = 0.5$			
			$A_{D-N}^s \times 100$			$\left \frac{A_{D-N}^C}{A_{D-N}^N} \right $	$A_{D-N}^s \times 100$			$\left \frac{A_{D-N}^C}{A_{D-N}^N} \right $
			<i>Night</i>	<i>Core</i>	<i>Mantle</i>		<i>Night</i>	<i>Core</i>	<i>Mantle</i>	
1	0.0008	9×10^{-6}	-0.03	-0.28	-0.01	7.95	-0.04	-0.40	-0.01	8.95
2	0.0008	7×10^{-6}	-0.10	-0.84	-0.03	8.73	-0.11	-0.97	-0.03	9.13
3	0.0008	5×10^{-6}	-0.27	-1.33	-0.19	5.00	-0.26	-1.24	-0.19	4.73
4	0.0010	9×10^{-5}	0.01	0.01	0.01	1.05	0.01	0.00	0.01	0.35
5	0.0010	7×10^{-6}	-0.12	-1.00	-0.05	8.33	-0.13	-1.16	-0.05	8.74
6	0.0010	5×10^{-6}	-0.32	-1.60	-0.23	4.97	-0.32	-1.49	-0.23	4.70
7	0.0020	1×10^{-5}	-0.03	-0.22	-0.01	7.53	-0.04	-0.32	-0.01	8.63
8	0.0020	7×10^{-6}	-0.16	-1.45	-0.05	9.28	-0.17	-1.65	-0.05	9.67
9	0.0020	5×10^{-6}	-0.54	-2.48	-0.35	4.60	-0.52	-2.27	-0.35	4.34
10	0.0040	1×10^{-5}	0.08	0.51	0.04	6.69	0.10	0.77	0.04	7.92
11	0.0040	7×10^{-6}	-0.04	-0.32	-0.02	7.82	-0.03	-0.19	-0.02	6.19
12	0.0040	5×10^{-6}	-0.50	-1.85	-0.39	3.67	-0.48	-1.56	-0.39	3.23
13	0.0060	1×10^{-5}	0.34	2.42	0.16	7.13	0.44	3.62	0.16	8.29
14	0.0060	7×10^{-6}	0.46	3.92	0.16	8.53	0.54	4.94	0.16	9.13
15	0.0060	5×10^{-6}	0.24	2.28	0.06	9.43	0.26	2.46	0.06	9.60
16	0.0080	1×10^{-5}	0.77	5.43	0.36	7.10	0.98	8.04	0.36	8.17
17	0.0080	7×10^{-6}	1.36	11.13	0.48	8.16	1.56	13.41	0.48	8.57
18	0.0080	5×10^{-6}	1.72	9.63	1.01	5.60	1.71	9.50	1.01	5.57
19	0.0100	7×10^{-6}	2.65	20.50	0.95	7.73	3.01	24.18	0.95	8.04
20	0.0100	5×10^{-6}	3.97	19.50	2.52	4.91	3.92	18.92	2.52	4.83
21	0.0130	5×10^{-6}	8.62	36.74	5.75	4.26	8.47	35.38	5.75	4.18
22	0.3000	1.5×10^{-5}	10.42	14.34	10.09	1.38	10.60	16.52	10.09	1.56
23	0.3000	2×10^{-5}	7.25	9.23	7.09	1.27	7.34	10.20	7.09	1.39
24	0.3000	3×10^{-5}	4.52	5.50	4.44	1.22	4.55	5.78	4.44	1.27
25	0.3000	4×10^{-5}	3.14	3.87	3.07	1.23	3.15	4.00	3.07	1.27
26	0.4800	3×10^{-5}	5.69	6.70	5.60	1.18	5.71	6.94	5.60	1.22
27	0.4800	5×10^{-5}	2.83	3.42	2.78	1.21	2.84	3.49	2.78	1.23
28	0.5000	2×10^{-5}	9.08	10.22	8.97	1.13	9.13	10.96	8.97	1.20
29	0.5600	1×10^{-5}	21.89	27.70	21.38	1.27	22.05	29.57	21.38	1.34
30	0.6000	8×10^{-5}	1.35	1.61	1.34	1.19	1.38	1.64	1.34	1.19
31	0.7000	3×10^{-5}	6.26	7.11	6.18	1.14	6.28	7.29	6.18	1.16
32	0.7000	5×10^{-5}	3.22	3.81	3.18	1.18	3.22	3.85	3.18	1.19
33	0.7700	2×10^{-5}	9.56	9.63	9.56	1.01	9.57	9.87	9.56	1.03
34	0.8000	1.3×10^{-4}	0.54	0.65	0.50	1.20	0.54	0.67	0.50	1.24
35	0.9000	4×10^{-5}	4.34	5.02	4.29	1.16	4.35	5.06	4.29	1.16
36	0.9000	1×10^{-4}	1.10	1.30	1.09	1.18	1.11	1.31	1.09	1.18

TABLE V. D - N Asymmetries for the SNO Detector for $T_{e,th} = 7.5$ MeV, ES, $\nu_e \rightarrow \nu_{\mu(\tau)}$ transition

N.	$\sin^2 2\theta_V$	Δm^2 [eV ²]	$Y_e(\text{core}) = 0.467$				$Y_e(\text{core}) = 0.5$			
			$A_{D-N}^s \times 100$			$\left \frac{A_{D-N}^C}{A_{D-N}^N} \right $	$A_{D-N}^s \times 100$			$\left \frac{A_{D-N}^C}{A_{D-N}^N} \right $
			<i>Night</i>	<i>Core</i>	<i>Mantle</i>		<i>Night</i>	<i>Core</i>	<i>Mantle</i>	
1	0.0008	9×10^{-6}	-0.06	-0.39	-0.01	6.72	-0.07	-0.55	-0.01	8.22
2	0.0008	7×10^{-6}	-0.14	-1.23	-0.05	8.72	-0.15	-1.36	-0.05	8.98
3	0.0008	5×10^{-6}	-0.28	-1.28	-0.24	4.65	-0.27	-0.71	-0.24	2.58
4	0.0010	9×10^{-5}	0.01	0.01	0.00	1.14	0.01	0.01	0.00	1.19
5	0.0010	7×10^{-6}	-0.17	-1.47	-0.06	8.71	-0.18	-1.61	-0.06	8.97
6	0.0010	5×10^{-6}	-0.43	-1.58	-0.28	3.66	-0.39	-0.84	-0.28	2.16
7	0.0020	1×10^{-5}	-0.04	-0.33	-0.02	8.09	-0.05	-0.48	-0.02	9.16
8	0.0020	7×10^{-6}	-0.27	-1.86	-0.11	6.97	-0.28	-2.37	-0.11	8.52
9	0.0020	5×10^{-6}	-0.71	-2.32	-0.55	3.28	-0.68	-2.07	-0.55	3.06
10	0.0040	1×10^{-5}	0.08	0.63	0.03	8.02	0.10	0.93	0.03	9.09
11	0.0040	7×10^{-6}	-0.12	-0.90	-0.05	7.64	-0.11	-0.83	-0.05	7.40
12	0.0040	5×10^{-6}	-0.73	-2.24	-0.60	3.09	-0.69	-1.83	-0.60	2.64
13	0.0060	1×10^{-5}	0.40	3.14	0.16	7.89	0.52	4.61	0.16	8.89
14	0.0060	7×10^{-6}	0.50	4.37	0.16	8.72	0.56	5.09	0.16	9.05
15	0.0060	5×10^{-6}	0.05	1.05	-0.04	21.87	0.04	0.98	-0.04	23.09
16	0.0080	1×10^{-5}	0.93	7.18	0.38	7.72	1.21	10.39	0.38	8.62
17	0.0080	7×10^{-6}	1.64	13.37	0.57	8.15	1.81	15.08	0.57	8.33
18	0.0080	5×10^{-6}	1.71	7.29	1.22	4.25	1.63	6.31	1.22	3.87
19	0.0100	7×10^{-6}	3.29	24.99	1.17	7.61	3.57	27.76	1.17	7.78
20	0.0100	5×10^{-6}	4.26	15.93	3.19	3.74	4.07	13.75	3.19	3.38
21	0.0130	5×10^{-6}	9.60	31.69	7.49	3.30	9.20	27.53	7.49	2.99
22	0.3000	1.5×10^{-5}	12.33	17.15	11.90	1.39	12.56	19.93	11.90	1.59
23	0.3000	2×10^{-5}	8.56	11.39	8.31	1.33	8.69	12.85	8.31	1.48
24	0.3000	3×10^{-5}	5.31	6.39	5.21	1.20	5.35	6.78	5.21	1.27
25	0.3000	4×10^{-5}	3.81	4.71	3.73	1.24	3.82	4.91	3.73	1.28
26	0.4800	3×10^{-5}	6.62	7.66	6.54	1.16	6.65	8.03	6.54	1.21
27	0.4800	5×10^{-5}	3.47	4.18	3.42	1.21	3.48	4.29	3.42	1.23
28	0.5000	2×10^{-5}	10.54	12.02	10.41	1.14	10.61	12.98	10.41	1.22
29	0.5600	1×10^{-5}	25.97	35.25	25.13	1.36	26.16	37.39	25.13	1.43
30	0.6000	8×10^{-5}	1.78	2.10	1.74	1.18	1.77	2.12	1.74	1.19
31	0.7000	3×10^{-5}	7.24	8.03	7.19	1.11	7.27	8.23	7.19	1.13
32	0.7000	5×10^{-5}	3.88	4.57	3.82	1.18	3.88	4.64	3.82	1.20
33	0.7700	2×10^{-5}	10.92	10.64	10.97	0.97	10.95	10.93	10.97	1.00
34	0.8000	1.3×10^{-4}	0.75	0.94	0.75	1.25	0.76	0.94	0.75	1.23
35	0.9000	4×10^{-5}	5.10	5.88	5.05	1.15	5.10	5.88	5.05	1.15
36	0.9000	1×10^{-4}	1.39	1.60	1.38	1.15	1.39	1.61	1.38	1.15

TABLE VI. D - N Asymmetries for the SNO Detector for $T_{e,th} = 5$ MeV, CC, $\nu_e \rightarrow \nu_s$ transition

N.	$\sin^2 2\theta_V$	Δm^2 [eV ²]	$Y_e(\text{core}) = 0.467$				$Y_e(\text{core}) = 0.5$			
			$A_{D-N}^s \times 100$			$\left \frac{A_{D-N}^C}{A_{D-N}^N} \right $	$A_{D-N}^s \times 100$			$\left \frac{A_{D-N}^C}{A_{D-N}^N} \right $
			<i>Night</i>	<i>Core</i>	<i>Mantle</i>		<i>Night</i>	<i>Core</i>	<i>Mantle</i>	
1	0.001	3×10^{-6}	-0.16	-0.69	-0.12	4.28	-0.17	-0.98	-0.12	5.76
2	0.001	5×10^{-6}	-0.07	-0.17	-0.06	2.48	-0.08	-0.31	-0.06	3.76
3	0.001	7×10^{-6}	0.01	0.00	0.01	0.43	0.00	-0.04	0.01	10.11
4	0.002	3×10^{-6}	-0.31	-1.45	-0.21	4.76	-0.33	-1.75	-0.21	5.36
5	0.002	5×10^{-6}	-0.04	-0.16	-0.04	4.60	-0.05	-0.45	-0.04	9.87
6	0.002	7×10^{-6}	0.00	0.03	-0.02	17.77	-0.02	-0.02	-0.02	1.24
7	0.002	8×10^{-6}	-0.02	-0.02	-0.01	1.27	-0.02	-0.06	-0.01	3.78
8	0.003	3×10^{-6}	-0.42	-1.89	-0.29	4.56	-0.44	-2.35	-0.29	5.30
9	0.003	5×10^{-6}	-0.06	-0.17	-0.05	3.03	-0.08	-0.53	-0.05	6.48
10	0.003	7×10^{-6}	-0.01	-0.03	-0.01	2.04	-0.02	-0.03	-0.01	1.95
11	0.004	4×10^{-6}	-0.20	-0.96	-0.14	4.72	-0.25	-1.59	-0.14	6.29
12	0.004	5×10^{-6}	-0.05	-0.18	-0.04	3.37	-0.08	-0.49	-0.04	6.24
13	0.005	4×10^{-6}	-0.19	-0.89	-0.13	4.76	-0.23	-1.44	-0.13	6.25
14	0.005	6×10^{-6}	0.01	0.06	0.00	10.67	0.01	0.05	0.00	9.58
15	0.005	7×10^{-6}	0.02	0.06	0.02	2.81	0.03	0.14	0.02	4.85
16	0.007	3.3×10^{-6}	-0.26	-1.28	-0.18	4.86	-0.28	-1.47	-0.18	5.30
17	0.007	4×10^{-6}	-0.06	-0.35	-0.03	6.01	-0.06	-0.35	-0.03	6.07
18	0.007	5×10^{-6}	0.08	0.06	0.08	0.70	0.10	0.29	0.08	2.91
19	0.007	6×10^{-6}	0.09	0.09	0.09	0.99	0.11	0.41	0.09	3.70
20	0.008	3×10^{-6}	-0.27	-1.13	-0.19	4.21	-0.26	-1.06	-0.19	4.04
21	0.008	4×10^{-6}	0.07	0.19	0.06	2.88	0.11	0.69	0.06	6.49
22	0.008	5×10^{-6}	0.13	0.20	0.12	1.55	0.18	0.85	0.12	4.71
23	0.008	6×10^{-6}	0.16	0.20	0.15	1.26	0.20	0.74	0.15	3.69
24	0.008	7×10^{-6}	0.18	0.41	0.18	2.27	0.23	1.02	0.18	4.47
25	0.009	3×10^{-6}	-0.06	-0.17	-0.05	2.73	-0.04	0.18	-0.05	5.10
26	0.009	4×10^{-6}	0.24	0.95	0.18	3.92	0.34	2.12	0.18	6.32
27	0.009	5×10^{-6}	0.23	0.44	0.22	1.86	0.33	1.62	0.22	4.90
28	0.009	6×10^{-6}	0.25	0.29	0.25	1.15	0.31	1.18	0.25	3.76
29	0.010	3×10^{-6}	0.22	1.11	0.14	5.12	0.27	1.81	0.14	6.66
30	0.010	4×10^{-6}	0.47	1.93	0.35	4.10	0.64	3.96	0.35	6.23
31	0.010	5×10^{-6}	0.37	0.75	0.34	2.01	0.53	2.67	0.34	5.08
32	0.014	4×10^{-6}	2.11	8.74	1.52	4.15	2.74	15.97	1.52	5.83
33	0.014	5×10^{-6}	1.37	2.98	1.23	2.17	1.94	9.81	1.23	5.06
34	0.400	6×10^{-6}	39.98	43.19	39.60	1.08	41.61	61.40	39.60	1.48
35	0.400	8×10^{-6}	29.78	53.96	27.27	1.81	32.07	73.33	27.27	2.29
36	0.400	1×10^{-5}	21.20	22.55	21.14	1.06	21.50	26.18	21.14	1.22
37	0.500	7×10^{-6}	32.45	55.71	30.09	1.72	34.52	73.63	30.09	2.13
38	0.500	8×10^{-6}	27.83	48.01	25.78	1.73	29.41	62.35	25.78	2.12
39	0.500	1×10^{-5}	20.01	19.46	20.05	0.97	20.11	21.64	20.05	1.08

TABLE VII. D - N Asymmetries for the SNO Detector for $T_{e,th} = 7.5$ MeV, CC, $\nu_e \rightarrow \nu_s$ transition

N.	$\sin^2 2\theta_V$	Δm^2 [eV ²]	$Y_e(\text{core}) = 0.467$				$Y_e(\text{core}) = 0.5$			
			$A_{D-N}^s \times 100$			$\left \frac{A_{D-N}^C}{A_{D-N}^N} \right $	$A_{D-N}^s \times 100$			$\left \frac{A_{D-N}^C}{A_{D-N}^N} \right $
			<i>Night</i>	<i>Core</i>	<i>Mantle</i>		<i>Night</i>	<i>Core</i>	<i>Mantle</i>	
1	0.001	3×10^{-6}	-0.18	-0.93	-0.13	5.14	-0.18	-0.98	-0.13	5.34
2	0.001	5×10^{-6}	-0.09	-0.23	-0.07	2.68	-0.10	-0.47	-0.07	4.48
3	0.001	7×10^{-6}	0.00	-0.01	0.00	1.60	-0.01	-0.05	0.00	5.32
4	0.002	3×10^{-6}	-0.39	-1.72	-0.25	4.36	-0.40	-1.67	-0.25	4.16
5	0.002	5×10^{-6}	-0.09	-0.36	-0.06	4.13	-0.12	-0.73	-0.06	6.14
6	0.002	7×10^{-6}	-0.01	-0.01	-0.02	0.93	-0.02	-0.07	-0.02	4.38
7	0.002	8×10^{-6}	-0.01	-0.04	-0.01	4.61	-0.01	-0.08	-0.01	6.51
8	0.003	3×10^{-6}	-0.50	-2.30	-0.36	4.56	-0.51	-2.43	-0.36	4.72
9	0.003	5×10^{-6}	-0.05	-0.40	-0.06	8.04	-0.09	-0.87	-0.06	9.63
10	0.003	7×10^{-6}	-0.02	0.01	-0.02	0.72	0.00	-0.04	-0.02	14.17
11	0.004	4×10^{-6}	-0.31	-1.53	-0.21	4.92	-0.37	-2.30	-0.21	6.20
12	0.004	5×10^{-6}	-0.09	-0.39	-0.06	4.53	-0.13	-0.87	-0.06	6.82
13	0.005	4×10^{-6}	-0.30	-1.48	-0.20	4.88	-0.36	-2.21	-0.20	6.13
14	0.005	6×10^{-6}	-0.01	0.00	-0.01	0.48	-0.01	-0.10	-0.01	6.71
15	0.005	7×10^{-6}	0.01	0.00	0.01	0.24	0.01	0.05	0.01	3.79
16	0.007	3.3×10^{-6}	-0.44	-2.01	-0.31	4.57	-0.46	-2.30	-0.31	4.97
17	0.007	4×10^{-6}	-0.14	-0.69	-0.09	4.93	-0.16	-0.89	-0.09	5.66
18	0.007	5×10^{-6}	0.03	0.07	0.03	2.13	0.05	0.30	0.03	5.87
19	0.007	6×10^{-6}	0.06	-0.02	0.07	0.25	0.08	0.22	0.07	2.67
20	0.008	3×10^{-6}	-0.46	-1.99	-0.33	4.30	-0.46	-2.02	-0.33	4.37
21	0.008	4×10^{-6}	0.02	0.09	0.01	4.72	0.04	0.33	0.01	8.69
22	0.008	5×10^{-6}	0.12	0.34	0.10	2.84	0.19	1.18	0.10	6.30
23	0.008	6×10^{-6}	0.13	-0.01	0.14	0.10	0.16	0.49	0.14	2.97
24	0.008	7×10^{-6}	0.16	0.15	0.16	0.92	0.19	0.49	0.16	2.57
25	0.009	3×10^{-6}	-0.27	-1.12	-0.20	4.14	-0.27	-1.07	-0.20	4.02
26	0.009	4×10^{-6}	0.24	1.15	0.16	4.80	0.31	2.03	0.16	6.57
27	0.009	5×10^{-6}	0.24	0.75	0.20	3.09	0.37	2.35	0.20	6.34
28	0.009	6×10^{-6}	0.21	-0.01	0.23	0.04	0.28	0.83	0.23	3.02
29	0.010	3×10^{-6}	0.00	0.07	0.00	15.49	0.02	0.21	0.00	13.41
30	0.010	4×10^{-6}	0.53	2.53	0.35	4.79	0.67	4.21	0.35	6.33
31	0.010	5×10^{-6}	0.40	1.25	0.33	3.11	0.61	3.93	0.33	6.45
32	0.014	4×10^{-6}	2.56	11.73	1.73	4.58	3.14	18.22	1.73	5.80
33	0.014	5×10^{-6}	1.52	4.91	1.22	3.23	2.27	13.77	1.22	6.05
34	0.400	6×10^{-6}	43.48	-0.62	46.33	0.01	43.30	-4.53	46.33	0.10
35	0.400	8×10^{-6}	35.09	73.55	30.79	2.10	39.13	97.84	30.79	2.50
36	0.400	1×10^{-5}	24.79	30.38	24.30	1.23	25.36	36.81	24.30	1.45
37	0.500	7×10^{-6}	36.92	64.75	33.97	1.75	39.54	84.97	33.97	2.15
38	0.500	8×10^{-6}	32.68	65.78	29.14	2.01	35.54	85.87	29.14	2.42
39	0.500	1×10^{-5}	23.29	26.36	23.02	1.13	23.54	29.42	23.02	1.25

TABLE VIII. D - N Asymmetries for the SNO Detector for $T_{e,th} = 5$ MeV, ES, $\nu_e \rightarrow \nu_s$ transition

N.	$\sin^2 2\theta_V$	Δm^2 [eV ²]	$Y_e(\text{core}) = 0.467$				$Y_e(\text{core}) = 0.5$			
			$A_{D-N}^s \times 100$			$\left \frac{A_{D-N}^C}{A_{D-N}^N} \right $	$A_{D-N}^s \times 100$			$\left \frac{A_{D-N}^C}{A_{D-N}^N} \right $
			<i>Night</i>	<i>Core</i>	<i>Mantle</i>		<i>Night</i>	<i>Core</i>	<i>Mantle</i>	
1	0.001	3×10^{-6}	-0.15	-0.68	-0.11	4.63	-0.16	-0.77	-0.11	4.88
2	0.001	5×10^{-6}	-0.03	-0.11	-0.03	3.50	-0.04	-0.25	-0.03	5.76
3	0.001	7×10^{-6}	-0.01	-0.02	-0.01	2.47	-0.01	-0.05	-0.01	3.78
4	0.002	3×10^{-6}	-0.27	-1.24	-0.19	4.58	-0.30	-1.63	-0.19	5.47
5	0.002	5×10^{-6}	-0.04	-0.11	-0.03	2.70	-0.06	-0.36	-0.03	6.29
6	0.002	7×10^{-6}	-0.01	-0.03	-0.01	2.09	-0.02	-0.05	-0.01	3.08
7	0.002	8×10^{-6}	-0.01	-0.04	-0.01	3.52	-0.01	-0.05	-0.01	3.62
8	0.003	3×10^{-6}	-0.37	-1.68	-0.25	4.60	-0.40	-2.14	-0.25	5.37
9	0.003	5×10^{-6}	-0.05	-0.13	-0.04	2.66	-0.07	-0.41	-0.04	5.95
10	0.003	7×10^{-6}	-0.01	-0.02	-0.01	1.41	-0.01	-0.05	-0.01	3.47
11	0.004	4×10^{-6}	-0.16	-0.72	-0.11	4.54	-0.20	-1.29	-0.11	6.37
12	0.004	5×10^{-6}	-0.04	-0.13	-0.03	2.95	-0.06	-0.37	-0.03	5.89
13	0.005	4×10^{-6}	-0.15	-0.70	-0.10	4.77	-0.18	-1.17	-0.10	6.41
14	0.005	6×10^{-6}	0.01	0.03	0.01	2.94	0.01	0.07	0.01	5.20
15	0.005	7×10^{-6}	0.03	0.07	0.02	2.43	0.03	0.14	0.02	4.23
16	0.007	3.3×10^{-6}	-0.21	-1.03	-0.14	4.80	-0.22	-1.16	-0.14	5.17
17	0.007	4×10^{-6}	-0.03	-0.25	-0.01	8.53	-0.03	-0.21	-0.01	7.97
18	0.007	5×10^{-6}	0.06	0.08	0.06	1.19	0.09	0.35	0.06	4.07
19	0.007	6×10^{-6}	0.10	0.16	0.09	1.62	0.12	0.47	0.09	3.81
20	0.008	3×10^{-6}	-0.20	-0.87	-0.14	4.44	-0.18	-0.72	-0.14	3.93
21	0.008	4×10^{-6}	0.08	0.19	0.07	2.33	0.12	0.71	0.07	5.70
22	0.008	5×10^{-6}	0.14	0.24	0.13	1.67	0.19	0.89	0.13	4.60
23	0.008	6×10^{-6}	0.17	0.26	0.17	1.50	0.22	0.82	0.17	3.78
24	0.008	7×10^{-6}	0.22	0.45	0.20	2.08	0.26	1.04	0.20	3.95
25	0.009	3×10^{-6}	0.00	0.05	0.00	12.41	0.04	0.56	0.00	12.54
26	0.009	4×10^{-6}	0.24	0.83	0.19	3.42	0.33	1.97	0.19	5.93
27	0.009	5×10^{-6}	0.25	0.46	0.23	1.86	0.34	1.62	0.23	4.81
28	0.009	6×10^{-6}	0.27	0.39	0.26	1.43	0.34	1.29	0.26	3.75
29	0.010	3×10^{-6}	0.27	1.27	0.18	4.69	0.35	2.24	0.18	6.42
30	0.010	4×10^{-6}	0.45	1.66	0.35	3.69	0.61	3.62	0.35	5.94
31	0.010	5×10^{-6}	0.38	0.73	0.35	1.90	0.53	2.57	0.35	4.85
32	0.014	4×10^{-6}	1.95	7.57	1.45	3.88	2.56	14.65	1.45	5.72
33	0.014	5×10^{-6}	1.38	2.85	1.25	2.07	1.91	9.33	1.25	4.87
34	0.400	6×10^{-6}	37.45	45.49	36.73	1.21	39.24	63.69	36.73	1.62
35	0.400	8×10^{-6}	27.32	46.97	25.39	1.72	29.17	63.58	25.39	2.18
36	0.400	1×10^{-5}	19.72	20.66	19.64	1.05	19.96	23.67	19.64	1.19
37	0.500	7×10^{-6}	30.09	50.42	28.08	1.68	31.91	66.54	28.08	2.09
38	0.500	8×10^{-6}	25.58	41.52	24.06	1.62	26.82	53.58	24.06	2.00
39	0.500	1×10^{-5}	18.66	18.78	18.64	1.01	18.76	20.14	18.64	1.07

TABLE IX. D - N Asymmetries for the SNO Detector for $T_{e,th} = 7.5$ MeV, ES, $\nu_e \rightarrow \nu_s$ transition

N.	$\sin^2 2\theta_V$	Δm^2 [eV ²]	$Y_e(\text{core}) = 0.467$				$Y_e(\text{core}) = 0.5$			
			$A_{D-N}^s \times 100$			$\left \frac{A_{D-N}^C}{A_{D-N}^N} \right $	$A_{D-N}^s \times 100$			$\left \frac{A_{D-N}^C}{A_{D-N}^N} \right $
			<i>Night</i>	<i>Core</i>	<i>Mantle</i>		<i>Night</i>	<i>Core</i>	<i>Mantle</i>	
1	0.001	3×10^{-6}	-0.17	-0.72	-0.13	4.20	-0.18	-1.01	-0.13	5.64
2	0.001	5×10^{-6}	-0.05	-0.18	-0.03	3.87	-0.06	-0.33	-0.03	5.43
3	0.001	7×10^{-6}	-0.01	-0.03	-0.01	2.01	-0.02	-0.06	-0.01	3.46
4	0.002	3×10^{-6}	-0.34	-1.61	-0.24	4.68	-0.36	-1.83	-0.24	5.08
5	0.002	5×10^{-6}	-0.04	-0.18	-0.02	4.63	-0.07	-0.52	-0.02	7.86
6	0.002	7×10^{-6}	-0.02	0.00	-0.01	0.02	-0.01	-0.07	-0.01	6.20
7	0.002	8×10^{-6}	-0.01	-0.04	0.00	2.66	-0.01	-0.06	0.00	6.32
8	0.003	3×10^{-6}	-0.46	-2.17	-0.33	4.68	-0.48	-2.45	-0.33	5.07
9	0.003	5×10^{-6}	-0.07	-0.27	-0.05	3.97	-0.10	-0.68	-0.05	6.78
10	0.003	7×10^{-6}	-0.02	-0.03	-0.02	1.62	-0.02	-0.06	-0.02	3.30
11	0.004	4×10^{-6}	-0.24	-1.17	-0.16	4.82	-0.30	-1.90	-0.16	6.32
12	0.004	5×10^{-6}	-0.07	-0.23	-0.05	3.56	-0.10	-0.63	-0.05	6.51
13	0.005	4×10^{-6}	-0.23	-1.11	-0.15	4.87	-0.28	-1.78	-0.15	6.34
14	0.005	6×10^{-6}	0.00	0.00	0.00	1.26	0.00	-0.04	0.00	9.71
15	0.005	7×10^{-6}	0.02	0.06	0.02	3.11	0.02	0.12	0.02	5.15
16	0.007	3.3×10^{-6}	-0.35	-1.60	-0.24	4.64	-0.37	-1.87	-0.24	5.11
17	0.007	4×10^{-6}	-0.09	-0.46	-0.06	5.15	-0.10	-0.55	-0.06	5.71
18	0.007	5×10^{-6}	0.04	0.02	0.04	0.56	0.06	0.27	0.04	4.44
19	0.007	6×10^{-6}	0.08	0.03	0.08	0.46	0.09	0.27	0.08	2.85
20	0.008	3×10^{-6}	-0.35	-1.52	-0.25	4.32	-0.36	-1.56	-0.25	4.40
21	0.008	4×10^{-6}	0.05	0.20	0.04	3.87	0.09	0.63	0.04	7.31
22	0.008	5×10^{-6}	0.12	0.23	0.11	1.89	0.18	0.96	0.11	5.32
23	0.008	6×10^{-6}	0.14	0.06	0.15	0.45	0.18	0.53	0.15	3.00
24	0.008	7×10^{-6}	0.19	0.37	0.17	1.96	0.23	0.92	0.17	3.93
25	0.009	3×10^{-6}	-0.15	-0.57	-0.11	3.86	-0.14	-0.43	-0.11	3.14
26	0.009	4×10^{-6}	0.25	1.11	0.17	4.48	0.34	2.22	0.17	6.59
27	0.009	5×10^{-6}	0.23	0.52	0.21	2.22	0.34	1.88	0.21	5.52
28	0.009	6×10^{-6}	0.23	0.10	0.24	0.45	0.29	0.88	0.24	3.07
29	0.010	3×10^{-6}	0.13	0.72	0.08	5.48	0.16	1.09	0.08	6.72
30	0.010	4×10^{-6}	0.50	2.27	0.35	4.52	0.66	4.24	0.35	6.38
31	0.010	5×10^{-6}	0.38	0.89	0.33	2.37	0.55	3.08	0.33	5.59
32	0.014	4×10^{-6}	2.31	10.20	1.60	4.42	2.95	17.41	1.60	5.90
33	0.014	5×10^{-6}	1.40	3.55	1.21	2.53	2.04	11.21	1.21	5.49
34	0.400	6×10^{-6}	41.82	32.96	42.52	0.79	42.86	46.73	42.52	1.09
35	0.400	8×10^{-6}	32.17	62.66	28.92	1.95	35.14	84.23	28.92	2.40
36	0.400	1×10^{-5}	22.78	24.64	22.62	1.08	23.14	28.95	22.62	1.25
37	0.500	7×10^{-6}	34.71	61.01	31.99	1.76	37.26	80.96	31.99	2.17
38	0.500	8×10^{-6}	30.04	56.07	27.38	1.87	32.09	72.80	27.38	2.27
39	0.500	1×10^{-5}	21.45	21.67	21.43	1.01	21.57	23.14	21.43	1.07

TABLE X. D - N Asymmetries for the SNO Detector for NC, $\nu_e \rightarrow \nu_s$ transition

N.	$\sin^2 2\theta_V$	Δm^2 [eV ²]	$Y_e(\text{core}) = 0.467$				$Y_e(\text{core}) = 0.5$			
			$A_{D-N}^s \times 100$			$\left \frac{A_{D-N}^C}{A_{D-N}^N} \right $	$A_{D-N}^s \times 100$			$\left \frac{A_{D-N}^C}{A_{D-N}^N} \right $
			<i>Night</i>	<i>Core</i>	<i>Mantle</i>		<i>Night</i>	<i>Core</i>	<i>Mantle</i>	
1	0.001	3×10^{-6}	-0.15	-0.68	-0.10	4.65	-0.16	-0.88	-0.10	5.67
2	0.001	5×10^{-6}	-0.03	-0.12	-0.03	3.59	-0.04	-0.24	-0.03	5.40
3	0.001	7×10^{-6}	-0.01	-0.02	-0.01	2.15	-0.01	-0.04	-0.01	3.06
4	0.002	3×10^{-6}	-0.27	-1.23	-0.19	4.53	-0.30	-1.58	-0.19	5.35
5	0.002	5×10^{-6}	-0.04	-0.12	-0.04	2.92	-0.06	-0.39	-0.04	6.40
6	0.002	7×10^{-6}	-0.01	-0.03	-0.01	1.98	-0.02	-0.05	-0.01	3.02
7	0.002	8×10^{-6}	-0.01	-0.03	-0.01	2.76	-0.01	-0.05	-0.01	3.82
8	0.003	3×10^{-6}	-0.37	-1.68	-0.26	4.56	-0.40	-2.08	-0.26	5.22
9	0.003	5×10^{-6}	-0.05	-0.12	-0.04	2.43	-0.07	-0.47	-0.04	6.39
10	0.003	7×10^{-6}	-0.01	-0.01	-0.01	1.17	-0.01	-0.04	-0.01	3.29
11	0.004	4×10^{-6}	-0.17	-0.79	-0.12	4.66	-0.21	-1.36	-0.12	6.34
12	0.004	5×10^{-6}	-0.05	-0.17	-0.04	3.58	-0.07	-0.38	-0.04	5.60
13	0.005	4×10^{-6}	-0.16	-0.77	-0.11	4.83	-0.20	-1.25	-0.11	6.36
14	0.005	6×10^{-6}	0.01	0.02	0.01	2.46	0.01	0.02	0.01	2.43
15	0.005	7×10^{-6}	0.03	0.07	0.02	2.43	0.03	0.14	0.02	4.32
16	0.007	3.3×10^{-6}	-0.23	-1.11	-0.16	4.79	-0.24	-1.25	-0.16	5.13
17	0.007	4×10^{-6}	-0.04	-0.30	-0.02	7.42	-0.04	-0.27	-0.02	7.08
18	0.007	5×10^{-6}	0.06	0.09	0.06	1.50	0.08	0.36	0.06	4.25
19	0.007	6×10^{-6}	0.10	0.13	0.09	1.37	0.12	0.42	0.09	3.51
20	0.008	3×10^{-6}	-0.22	-0.97	-0.15	4.47	-0.21	-0.84	-0.15	4.05
21	0.008	4×10^{-6}	0.08	0.18	0.07	2.36	0.12	0.68	0.07	5.83
22	0.008	5×10^{-6}	0.14	0.27	0.13	1.87	0.20	0.96	0.13	4.90
23	0.008	6×10^{-6}	0.17	0.22	0.16	1.29	0.21	0.74	0.16	3.55
24	0.008	7×10^{-6}	0.22	0.42	0.20	1.97	0.26	1.03	0.20	3.90
25	0.009	3×10^{-6}	-0.02	-0.09	-0.02	3.74	0.01	0.37	-0.02	29.98
26	0.009	4×10^{-6}	0.24	0.86	0.19	3.55	0.33	1.98	0.19	5.98
27	0.009	5×10^{-6}	0.25	0.52	0.23	2.07	0.35	1.73	0.23	4.98
28	0.009	6×10^{-6}	0.27	0.33	0.26	1.25	0.33	1.16	0.26	3.47
29	0.010	3×10^{-6}	0.24	1.09	0.16	4.59	0.31	1.97	0.16	6.38
30	0.010	4×10^{-6}	0.46	1.75	0.35	3.81	0.62	3.67	0.35	5.97
31	0.010	5×10^{-6}	0.39	0.86	0.35	2.18	0.55	2.75	0.35	5.02
32	0.014	4×10^{-6}	2.03	8.05	1.50	3.96	2.64	15.01	1.50	5.69
33	0.014	5×10^{-6}	1.43	3.29	1.27	2.31	1.99	10.06	1.27	5.05
34	0.400	6×10^{-6}	37.48	42.13	36.96	1.12	39.00	57.94	36.96	1.49
35	0.400	8×10^{-6}	27.62	49.35	25.50	1.79	29.64	66.96	25.50	2.26
36	0.400	1×10^{-5}	19.91	20.95	19.82	1.05	20.25	25.11	19.82	1.24
37	0.500	7×10^{-6}	29.95	50.13	28.16	1.67	31.75	66.58	28.16	2.10
38	0.500	8×10^{-6}	25.82	43.08	24.16	1.67	27.19	56.59	24.16	2.08
39	0.500	1×10^{-5}	18.72	17.64	18.81	0.94	18.88	19.64	18.81	1.04

FIGURE CAPTIONS

Figures 1a - 1f. The variation with Δm^2 and $\sin^2 2\theta_V$ of the difference between the values of the *Core (Night)* D-N asymmetry (a) - (c) ((d) - (f)), calculated utilizing the predictions for the relevant CC and NC reaction cross-sections derived in ref. [30] and in ref. [31]: figures (a), (b), (e) ((c), (f)) show the asymmetry difference in the one year averaged CC (NC) event rate; figures (a), (d) ((b), (c), (e) and (f)) correspond to $\nu_e \rightarrow \nu_{\mu(\tau)}$ ($\nu_e \rightarrow \nu_s$) transitions. The light-grey spot-like regions in the upper left-hand panels correspond to asymmetry differences exceeding 1%, while the dark-grey areas are the regions of the MSW solutions.

Figures 2a - 2b. The probabilities $\langle P_{e2} \rangle^C$ (solid line), $\langle P_{e2} \rangle^N$ (dashed line) and $\langle P_{e2} \rangle^M$ (dash-dotted line) as functions of $E/\Delta m^2$ for $\sin^2 2\theta_V = 0.005$ (a); 0.010 (b) in the case of $\nu_e \rightarrow \nu_{\mu(\tau)}$ transitions of solar neutrinos.

Figure 3. The dependence of P_{e2} on ρ_r and the Nadir angle \hat{h} for $\sin^2 2\theta_V = 0.01$ in the case of MSW $\nu_e \rightarrow \nu_{\mu(\tau)}$ (upper left panel) and $\nu_e \rightarrow \nu_s$ (upper right panel) transitions of solar neutrinos. The grey-scales correspond to different values of P_{e2} , as is indicated in the two vertical columns between the two upper panels. The thin solid lines in both upper panels represent contours of constant P_{e2} values: $P_{e2} = 0.01, 0.025, 0.05, 0.1, 0.15, 0.2, 0.25, 0.30, 0.40$. The dotted and the thick black lines are minimum gradient axes, connecting the points of local maxima of P_{e2} in the variable ρ_r at fixed \hat{h} (“ridges”), while the dash-dotted lines are minimum gradient axes connecting points of local minima of P_{e2} (“valleys”). The solid lines in the lower panels show P_{e2} as a function of \hat{h} , computed along the “ridge” leading to the absolute maximum of P_{e2} at $\hat{h} = 0^\circ$, while the dashed lines show the dependence of P_{e2} on \hat{h} along the $\rho_r = \text{const.}$ line (dashed lines in the upper panels) starting from the point of the absolute maximum at $\hat{h} = 0^\circ$.

Figures 4a - 4b, 5a - 5b. Iso - (D-N) asymmetry contour plots for the one year average CC *Night* (4a,4b), and *Core* (5a,5b) asymmetries for the SNO detector in the case of the $\nu_e \rightarrow \nu_{\mu(\tau)}$ transitions and $T_{e,th} = 5.0$ (a); 7.5 (b) MeV. The solid (dashed) lines correspond to $Y_e(\text{core}) = 0.467$ (0.500). The MSW SMA and LMA “conservative” solution regions from ref. [11] are also shown.

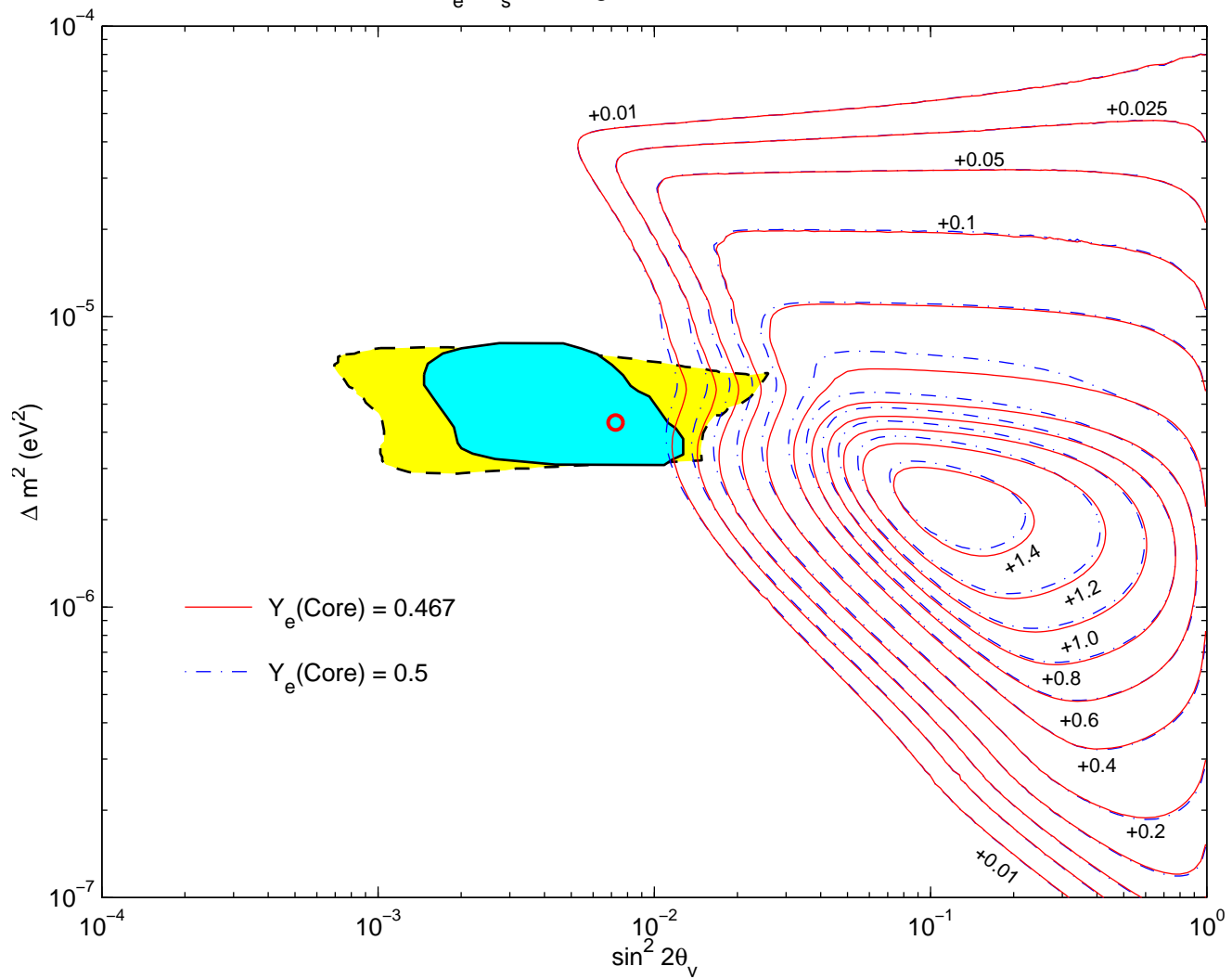
Figures 6a - 6b, 7a - 7b. Iso - (D-N) asymmetry contour plots for the one year average ES *Night* (6a,6b), and *Core* (7a,7b) asymmetries for the SNO detector in the case of the $\nu_e \rightarrow \nu_{\mu(\tau)}$ transitions and $T_{e,th} = 5.0$ (a); 7.5 (b) MeV. The solid (dashed) lines correspond to $Y_e(\text{core}) = 0.467$ (0.500). The MSW SMA and LMA “conservative” solution regions [11] are also shown.

Figures 8a - 8b, 9a - 9c. The same as in figures 4a - 4b and 5a - 5b in the case of the $\nu_e \rightarrow \nu_s$ transitions of solar neutrinos. The CC *Core* asymmetry in figures 9a - 9c correspond to $T_{e,th} = 5.0$ (a,b); 7.5 (c) and $Y_e(\text{core}) = 0.467$ (a,c); 0.500 (b). The MSW $\nu_e \rightarrow \nu_s$ transition solution regions from ref. [11] are also shown (the “conservative” solution region is marked with thin dashed lines).

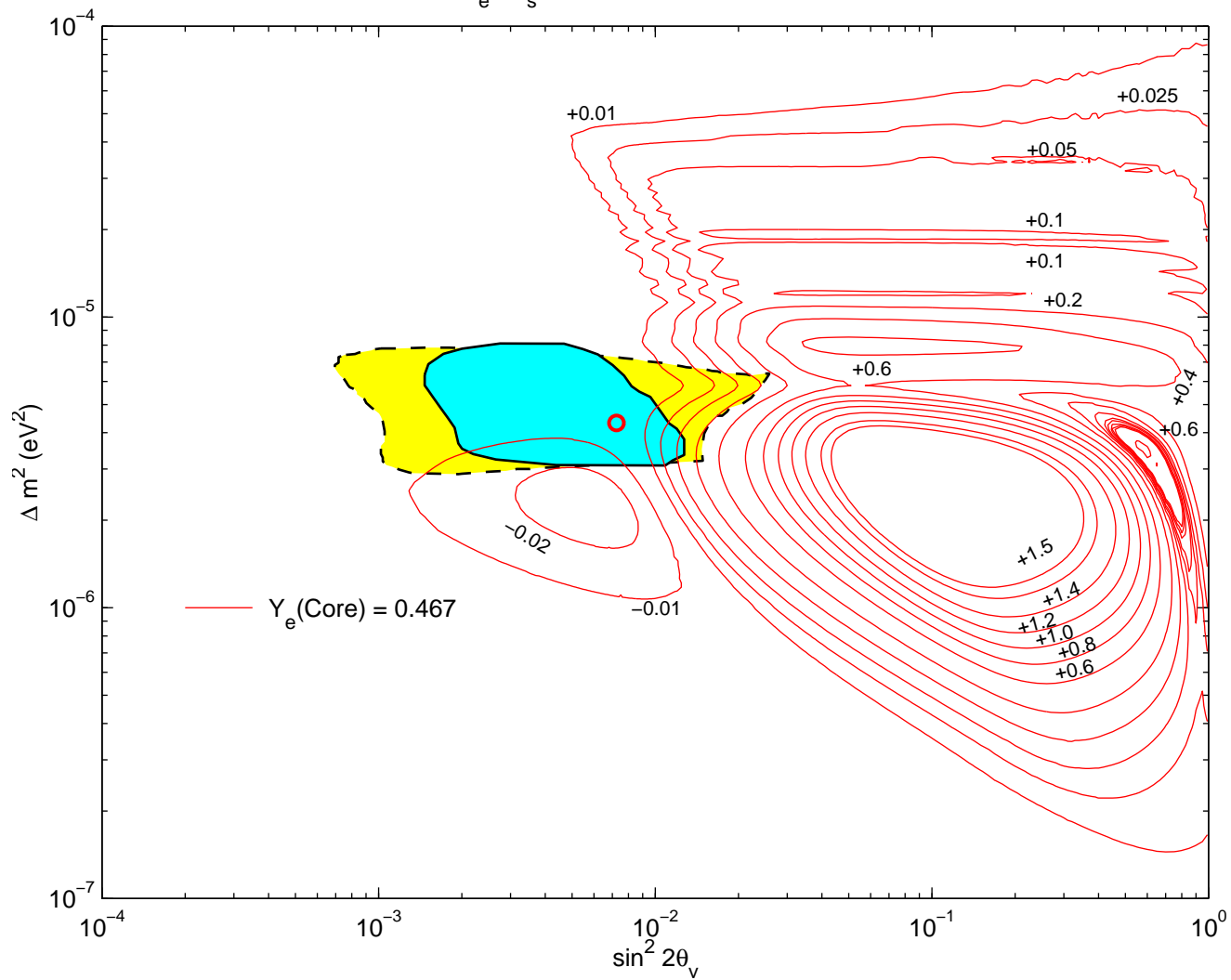
Figures 10a - 10b. Iso - (D-N) asymmetry contour plots for the one year average ES *Night* (a) and *Core* (b) asymmetries for the SNO detector in the case of the $\nu_e \rightarrow \nu_s$ transitions of solar neutrinos for $T_{e,th} = 5.0$ and $Y_e(\text{core}) = 0.467$. The MSW $\nu_e \rightarrow \nu_s$ transition solution regions [11] are also shown (the “conservative” solution region is marked with thin dashed lines).

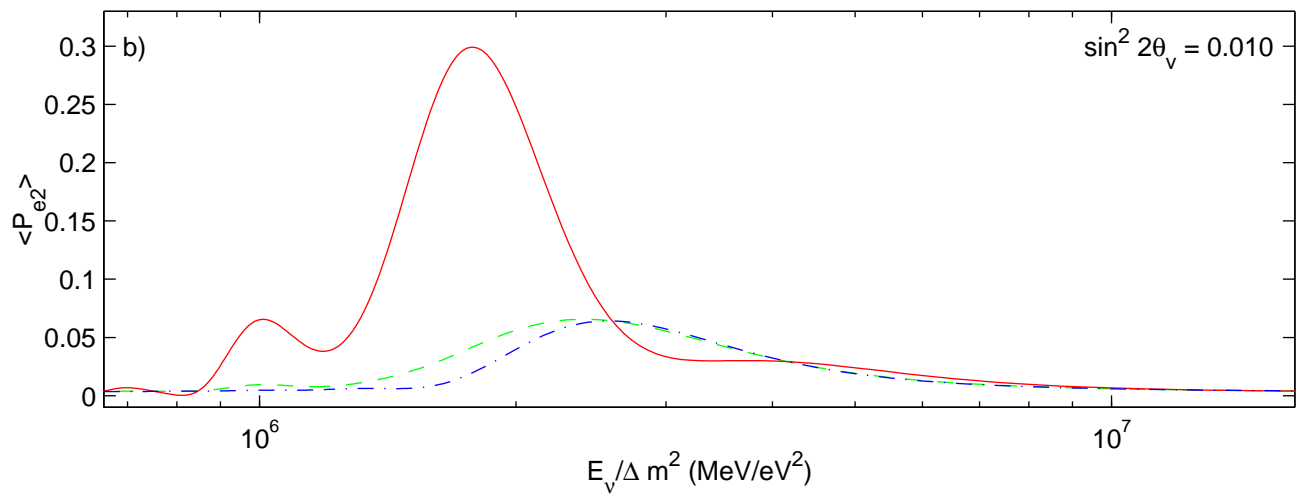
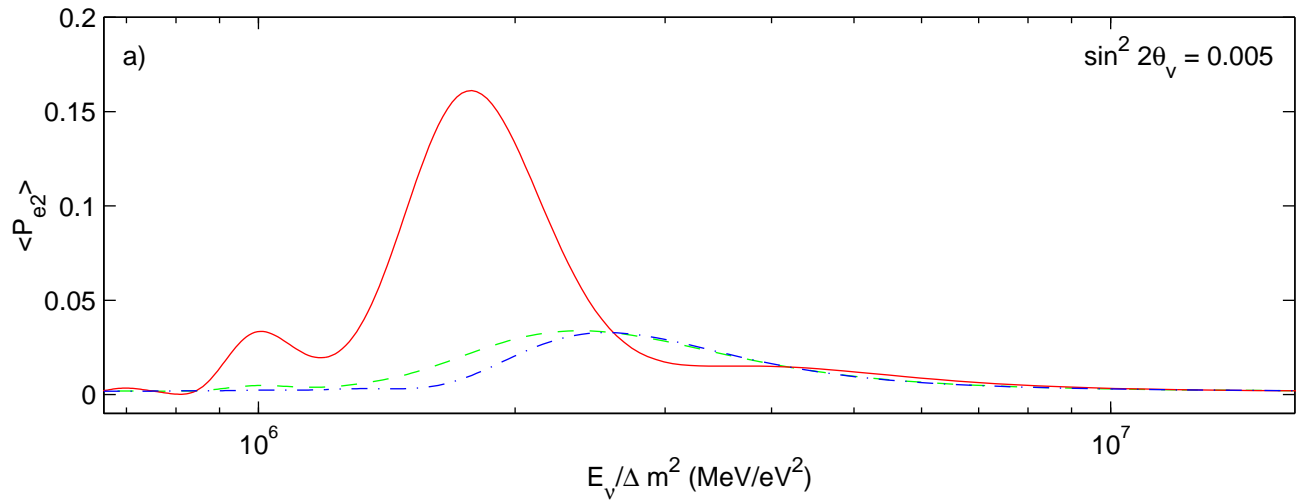
Figures 11a - 11b. The same as in Fig. 10 for the one year average NC *Night* (a) and *Core* (b) asymmetries in the case of the $\nu_e \rightarrow \nu_s$ transitions of solar neutrinos. The solid (dashed) lines correspond to $Y_e(\text{core}) = 0.467$ (0.500).

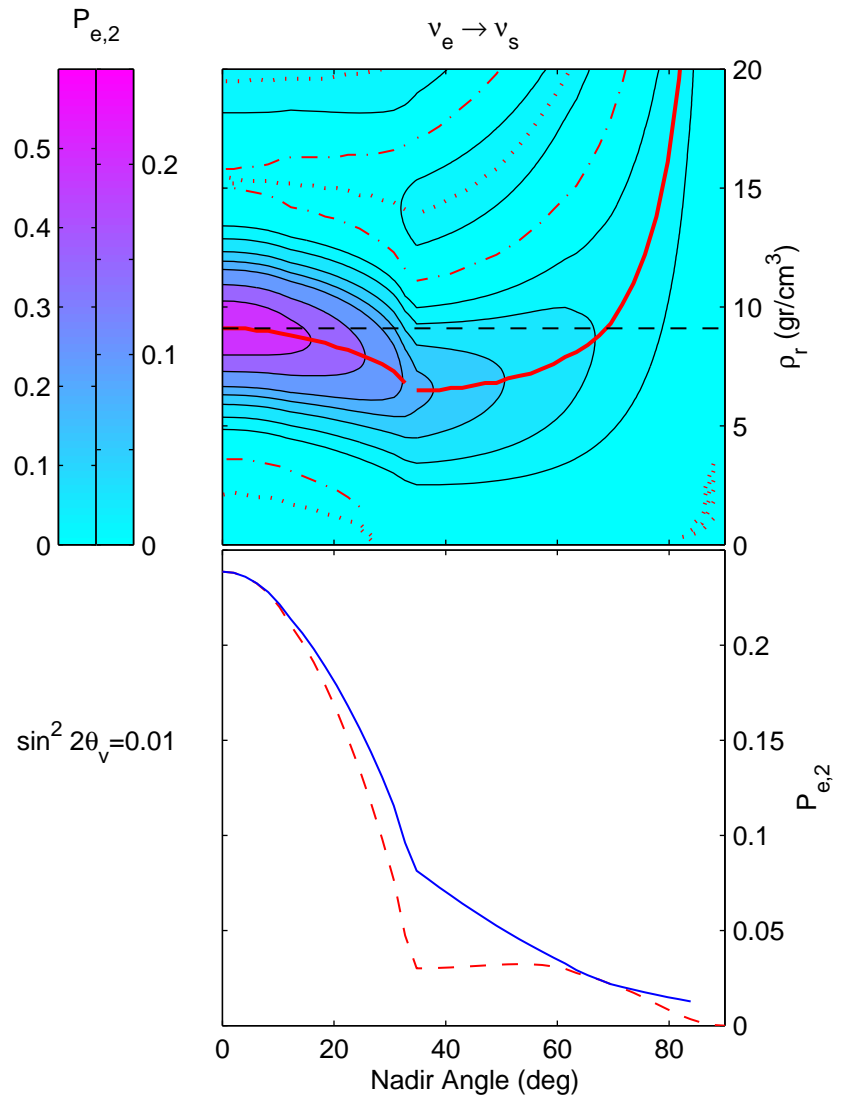
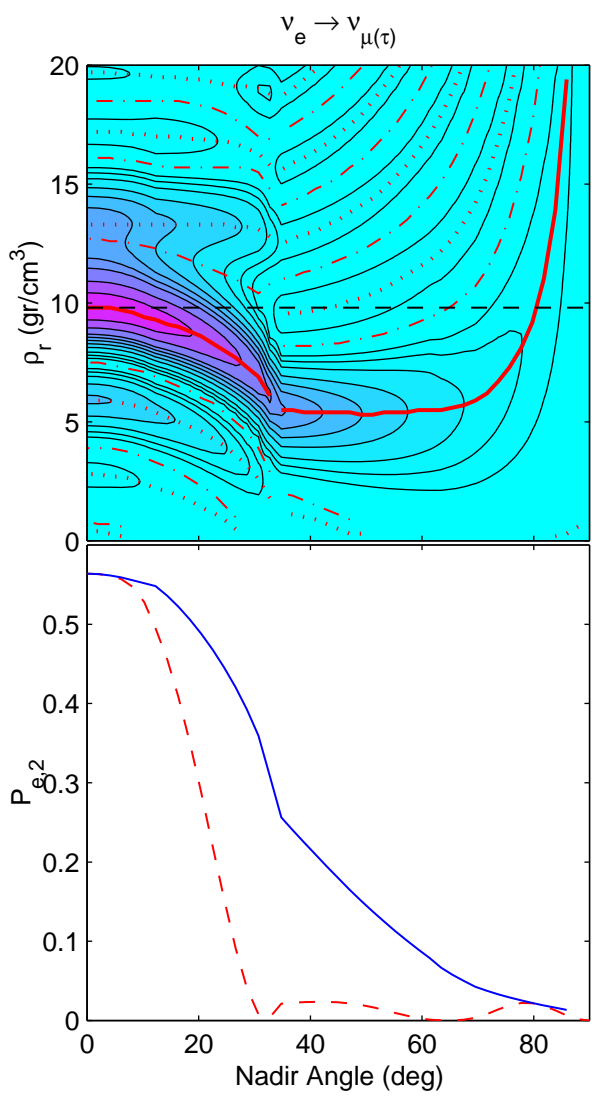
$\nu_e \rightarrow \nu_s$, Full Night, SNO Neutral Current

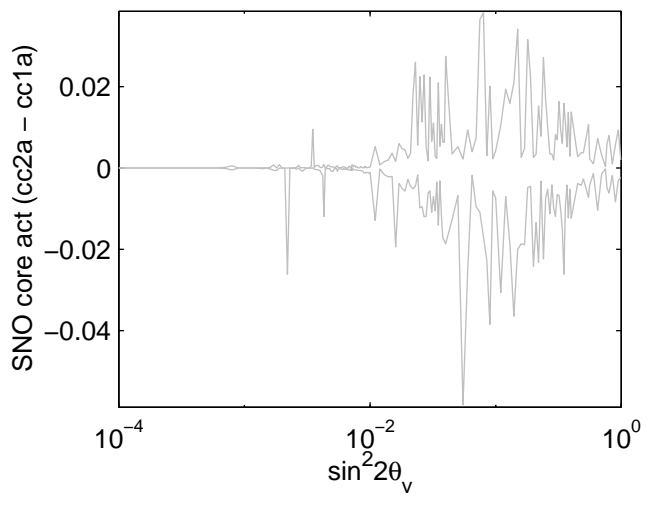
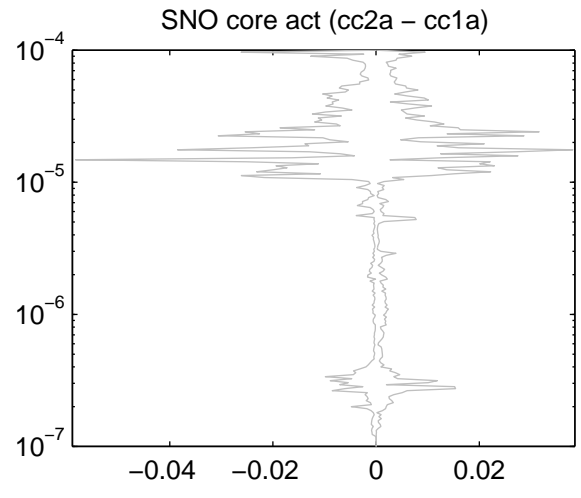
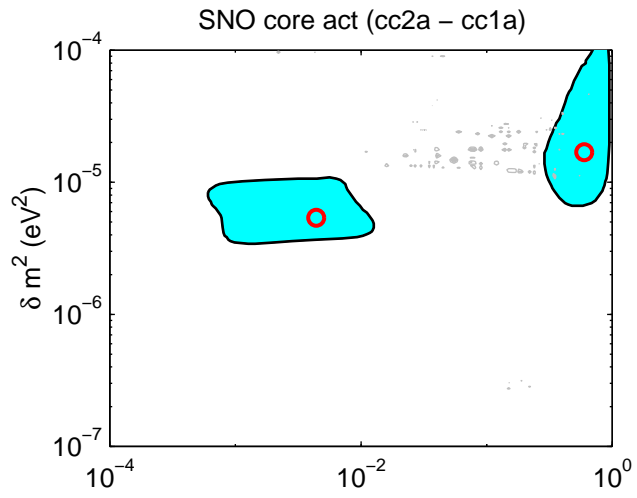


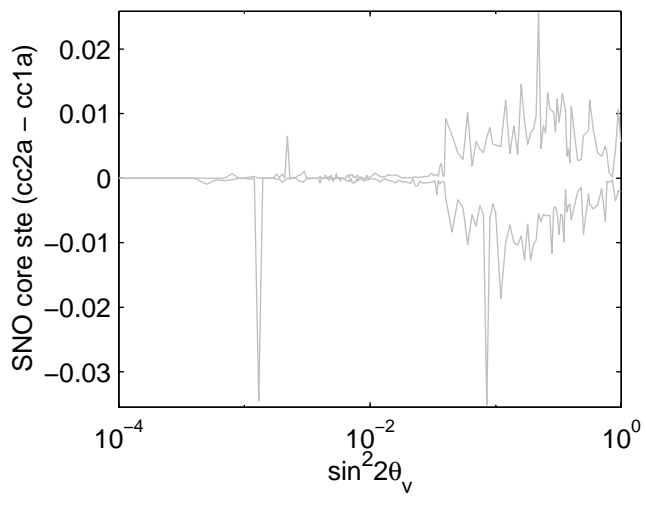
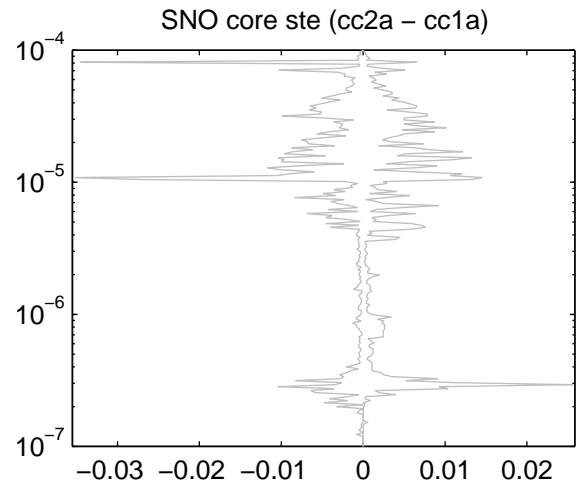
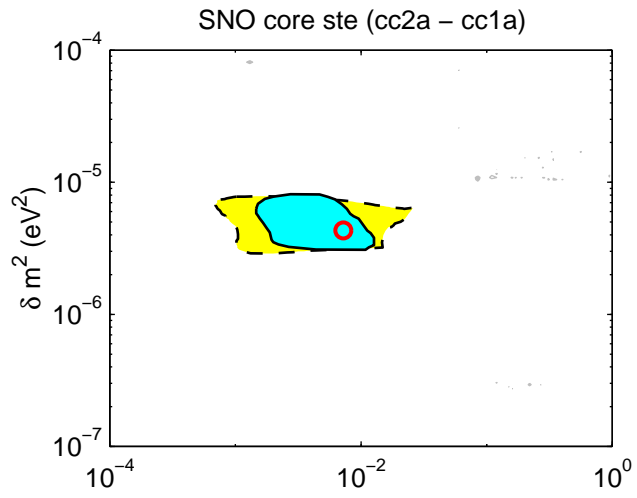
$\nu_e \rightarrow \nu_s$, Core, SNO Neutral Current

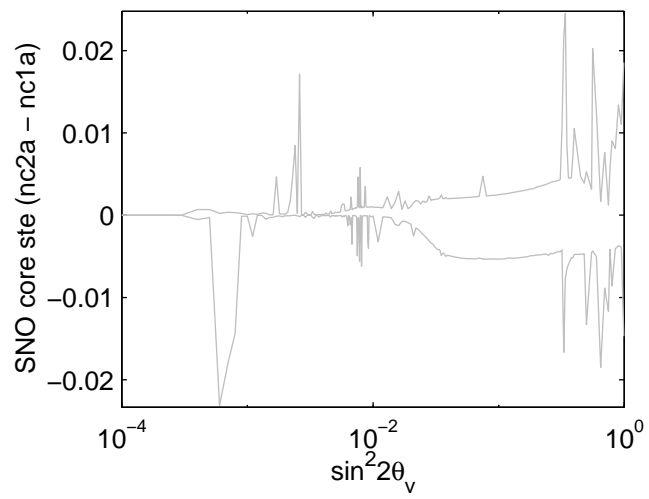
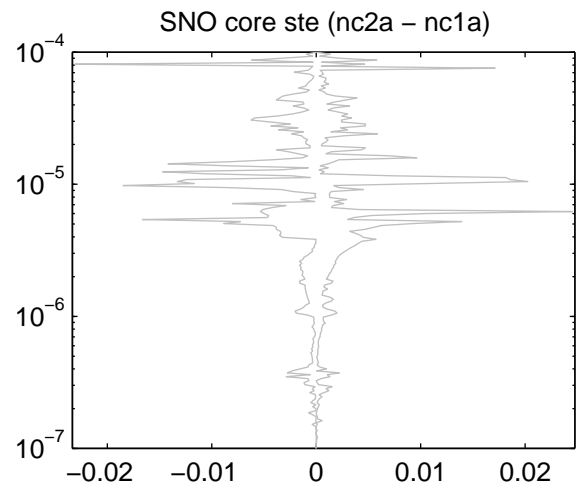
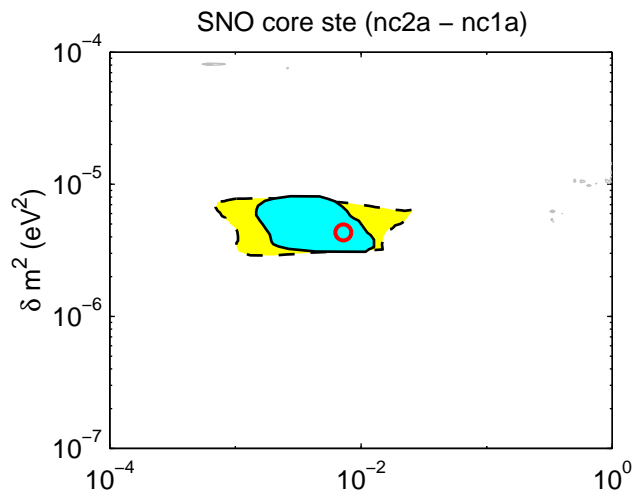


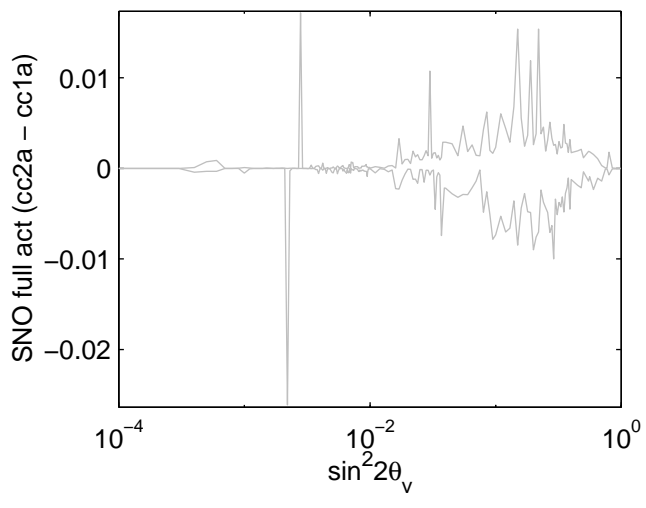
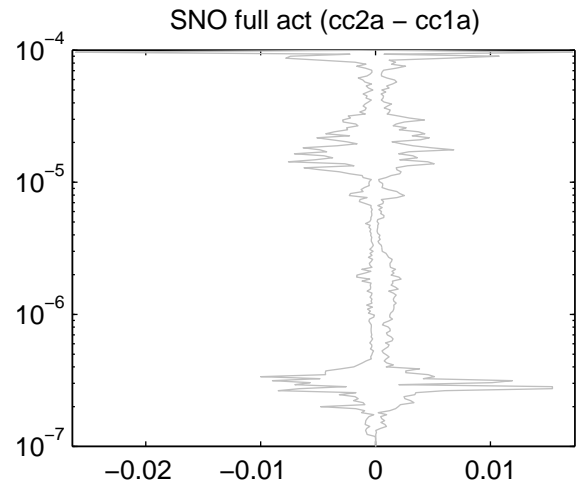
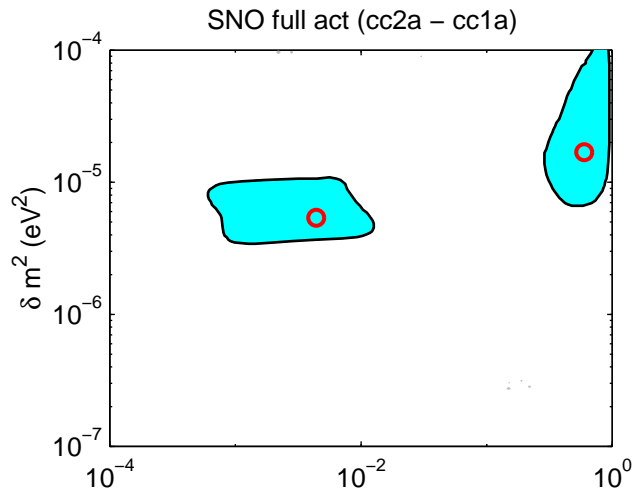


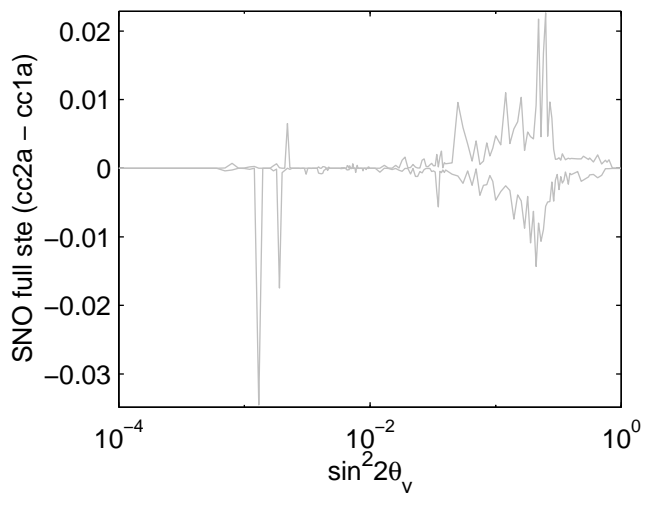
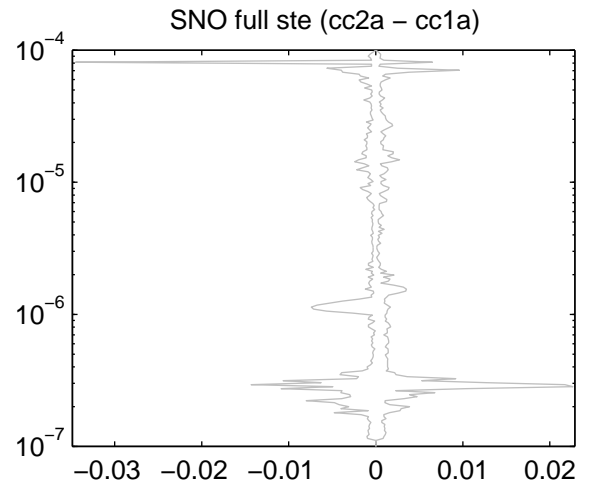
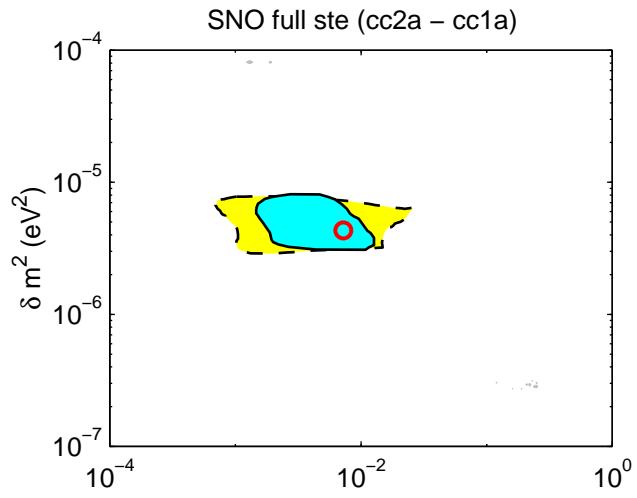


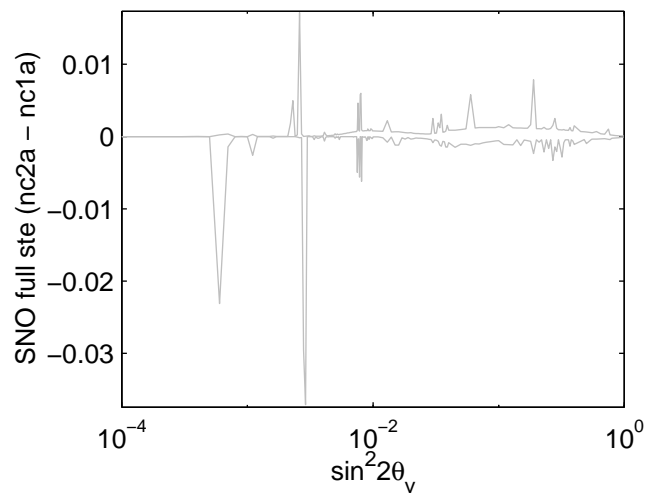
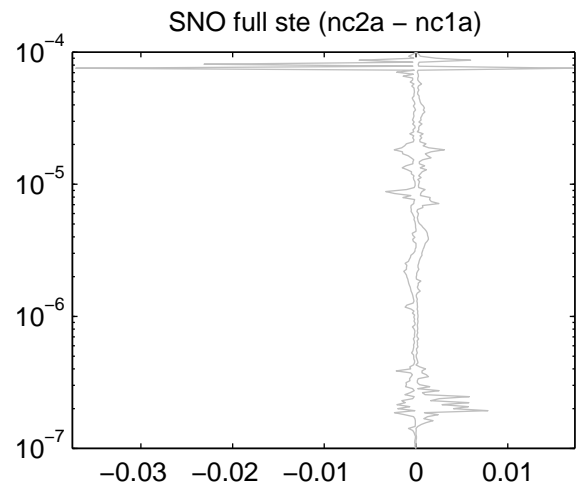
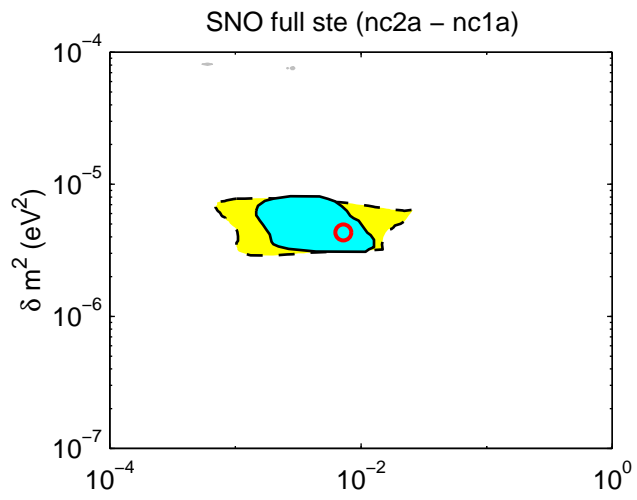




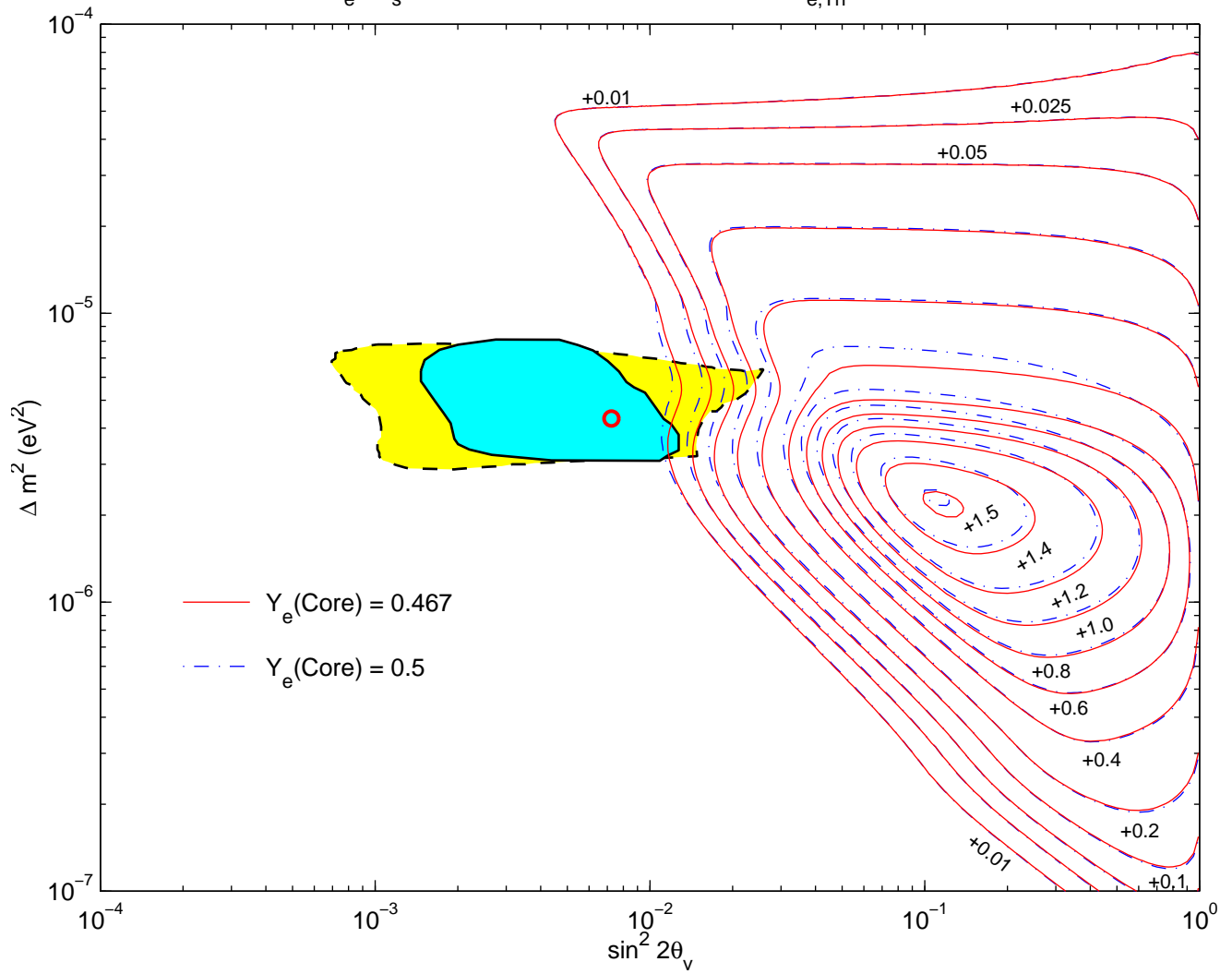




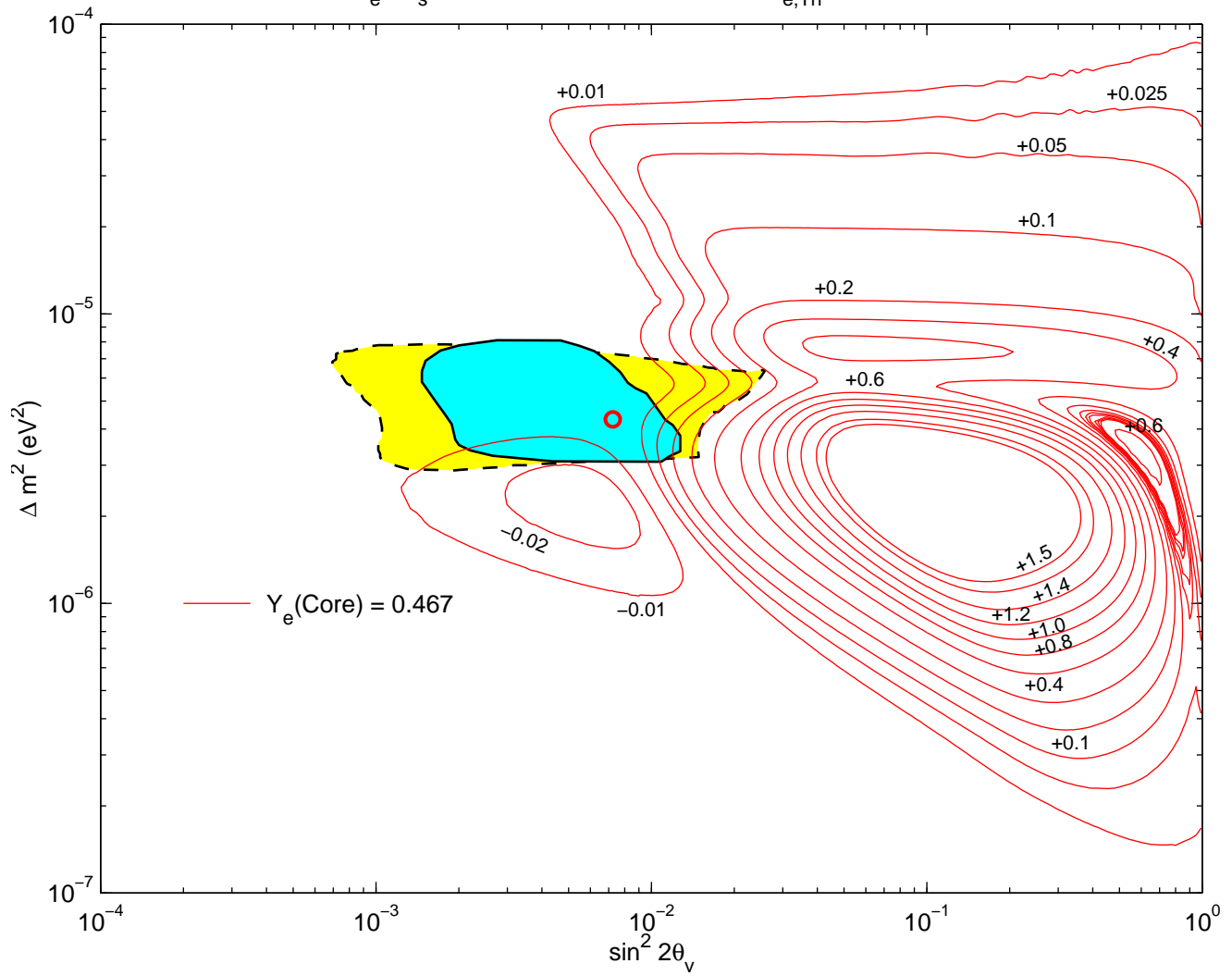




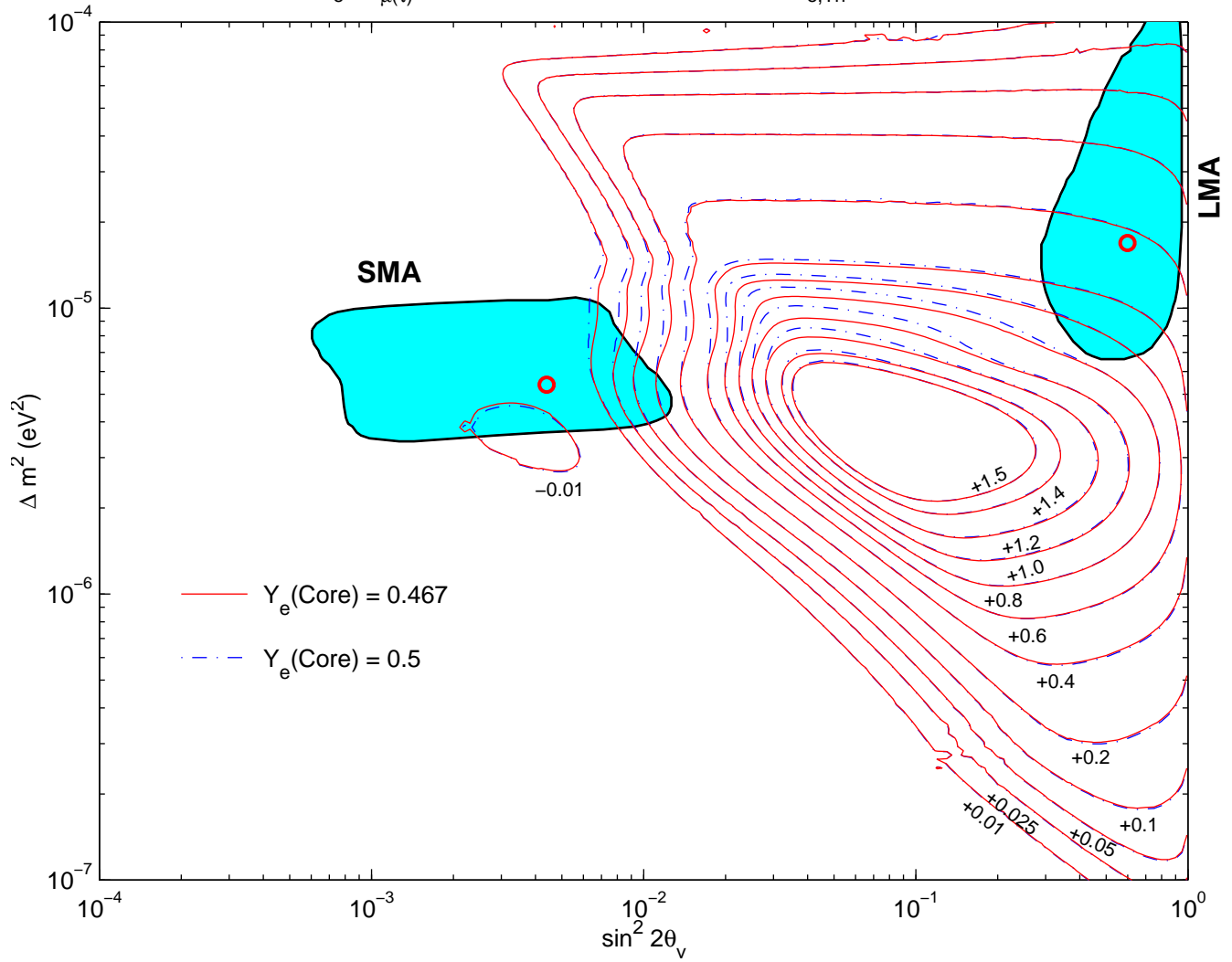
$\nu_e \rightarrow \nu_s$, Full Night, SNO Elastic Scattering ($T_{e,Th} = 5.0$ MeV)



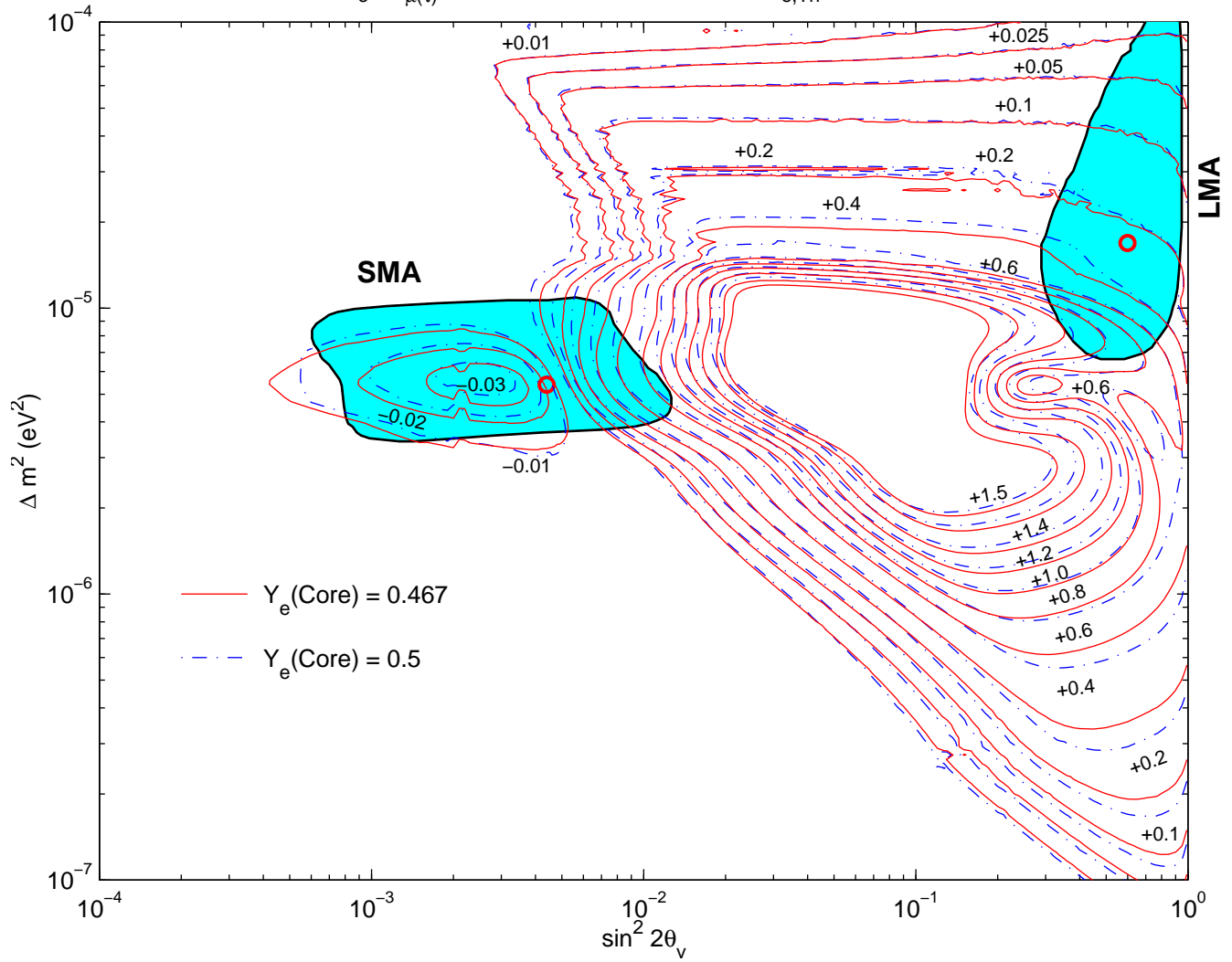
$\nu_e \rightarrow \nu_{s'}$, Core, SNO Elastic Scattering ($T_{e,Th} = 5.0$ MeV)



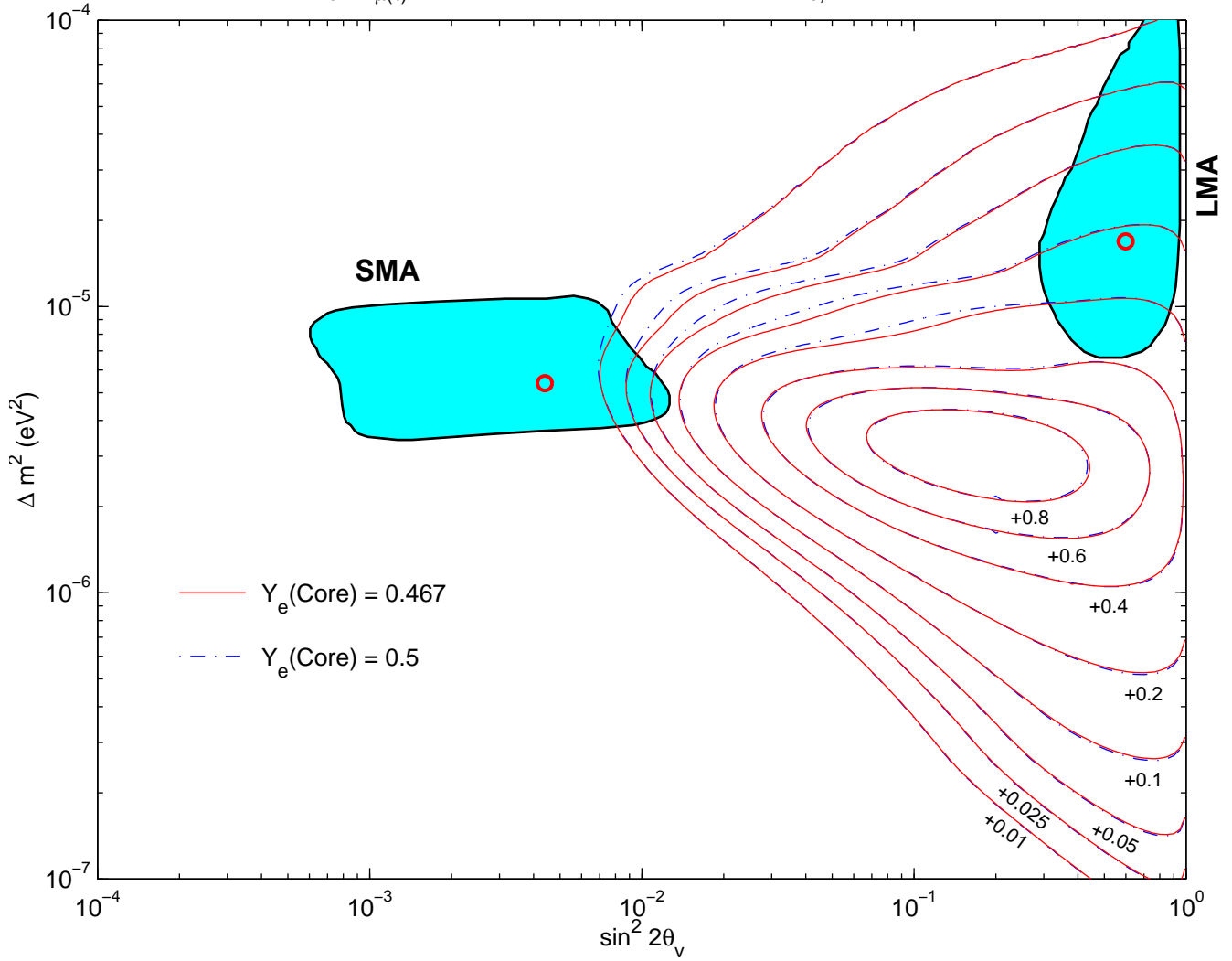
$\nu_e \rightarrow \nu_{\mu(\tau)}$, Full Night, SNO Charged Current ($T_{e, Th} = 5.0$ MeV)



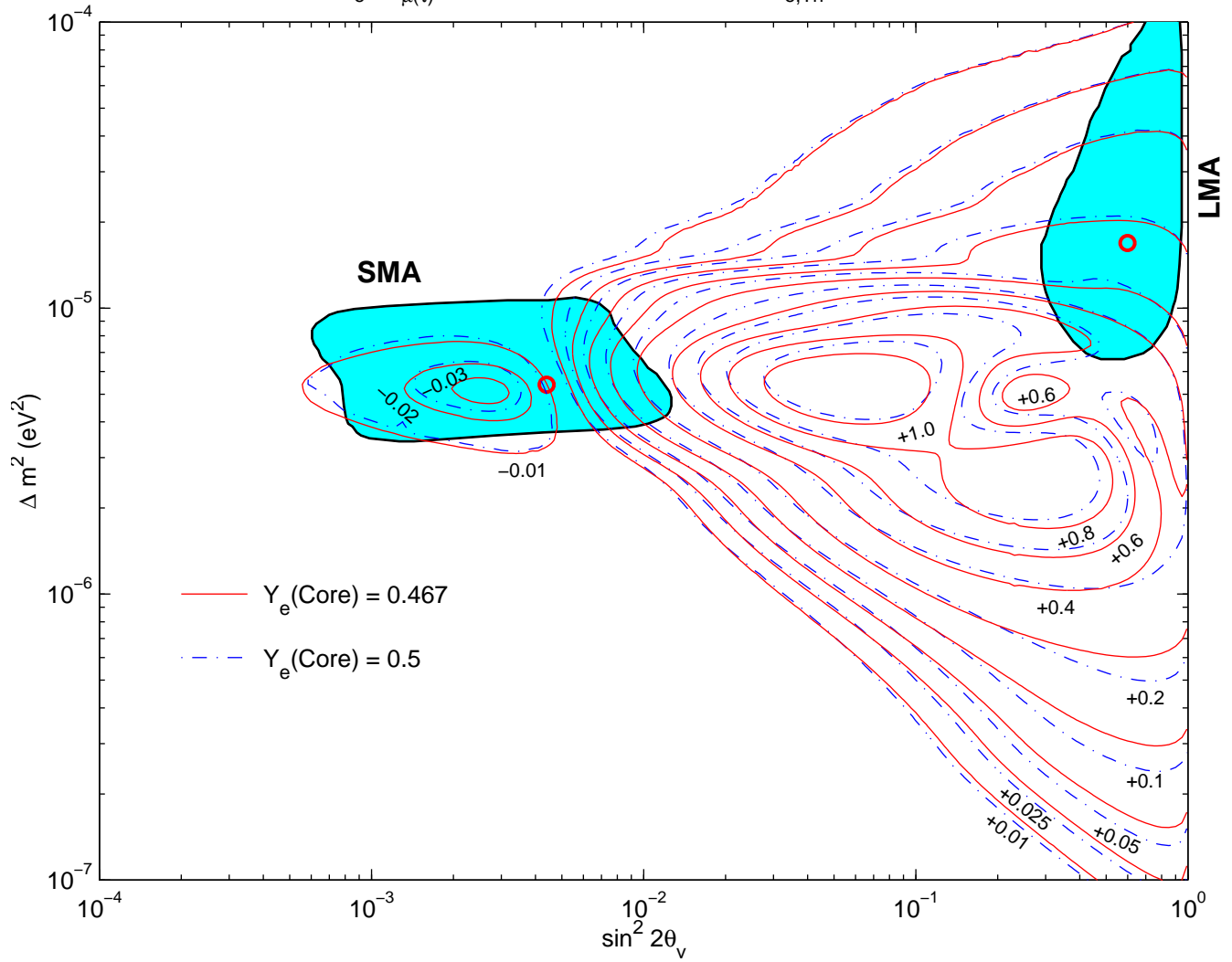
$\nu_e \rightarrow \nu_{\mu(\tau)}$, Core, SNO Charged Current ($T_{e, \text{Th}} = 5.0 \text{ MeV}$)



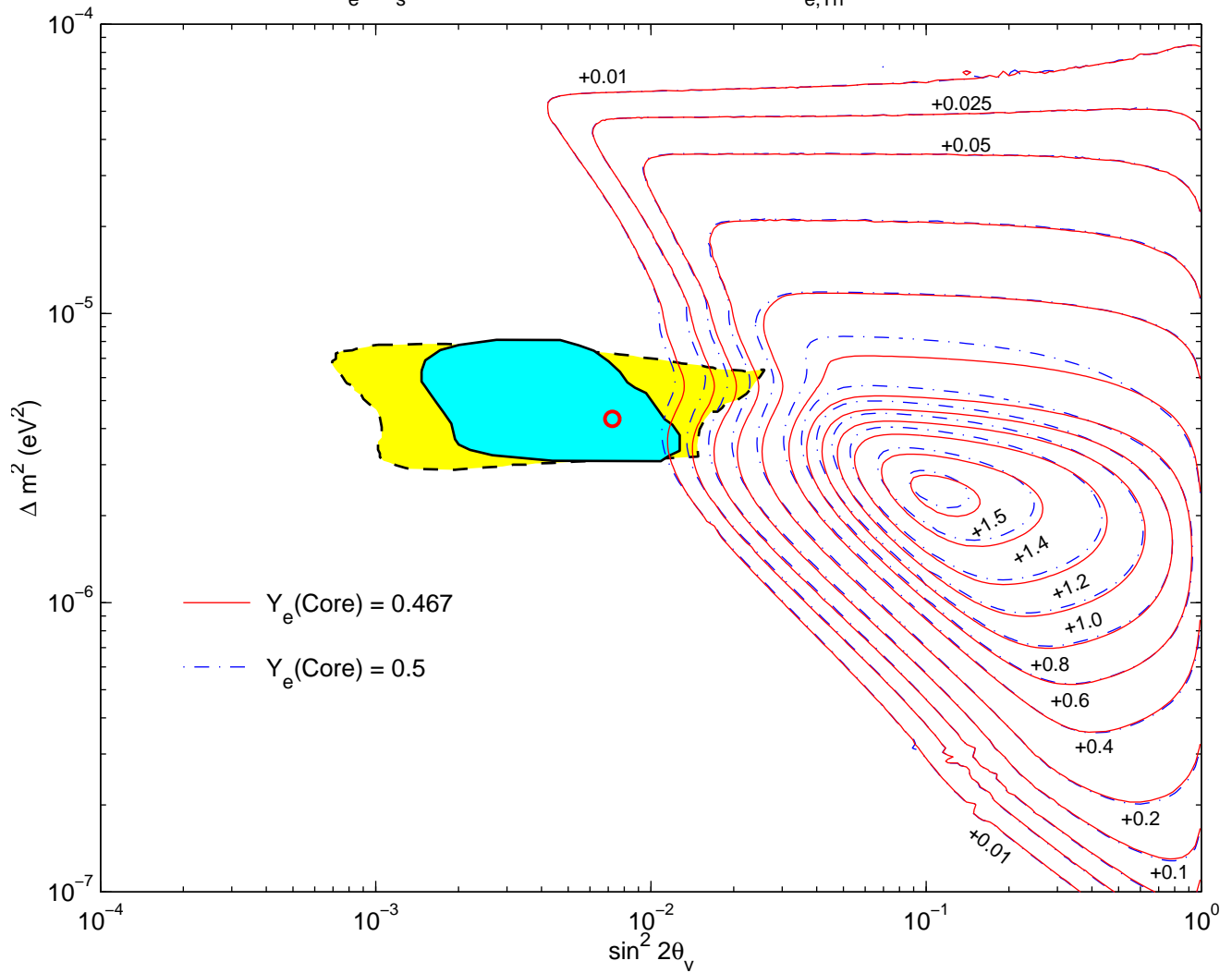
$\nu_e \rightarrow \nu_{\mu(\tau)}$, Full Night, SNO Elastic Scattering ($T_{e,Th} = 5.0$ MeV)



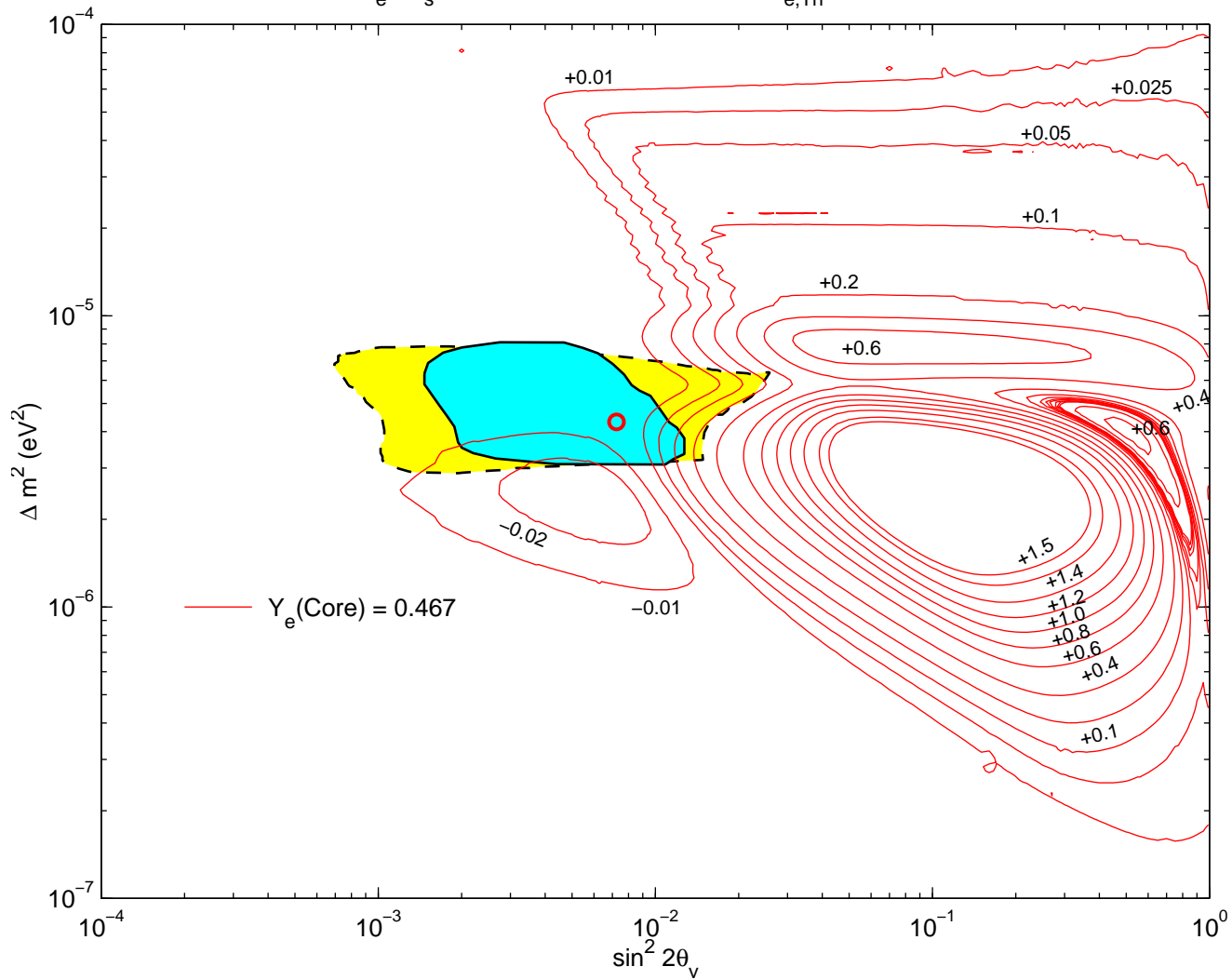
$\nu_e \rightarrow \nu_{\mu(\tau)}$, Core, SNO Elastic Scattering ($T_{e,Th} = 5.0$ MeV)



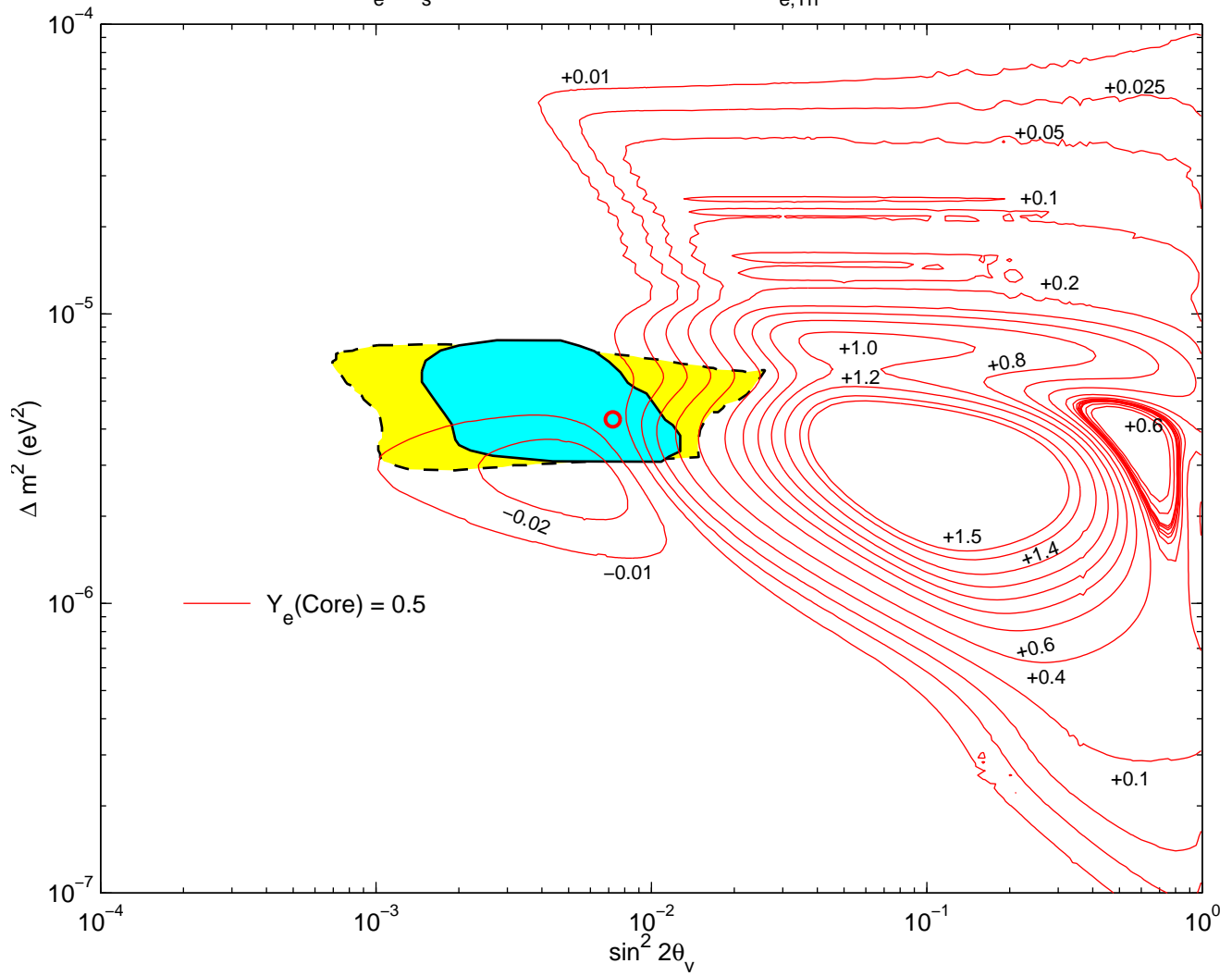
$\nu_e \rightarrow \nu_s$, Full Night, SNO Charged Current ($T_{e,Th} = 5.0$ MeV)



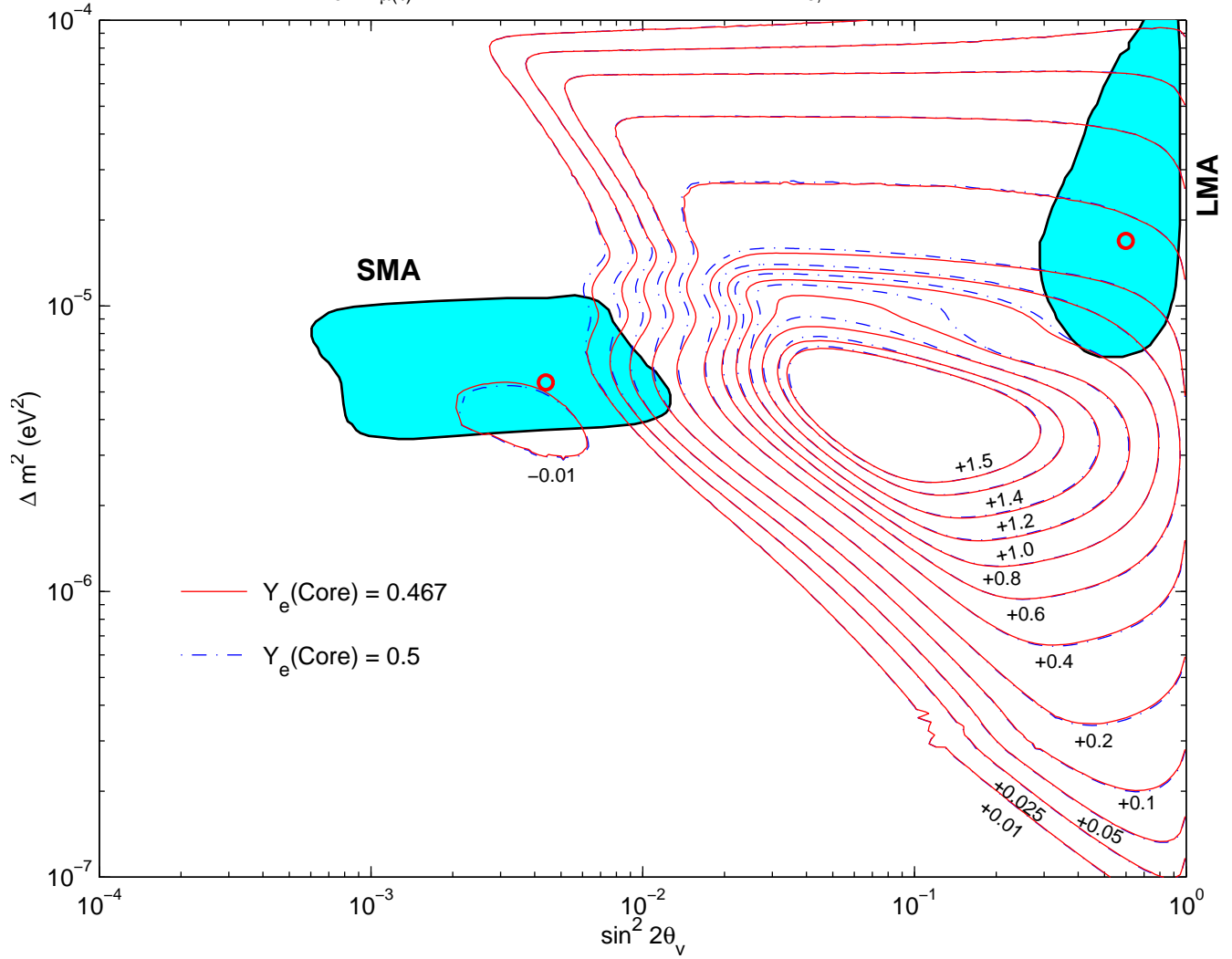
$\nu_e \rightarrow \nu_s$, Core, SNO Charged Current ($T_{e,Th} = 5.0$ MeV)



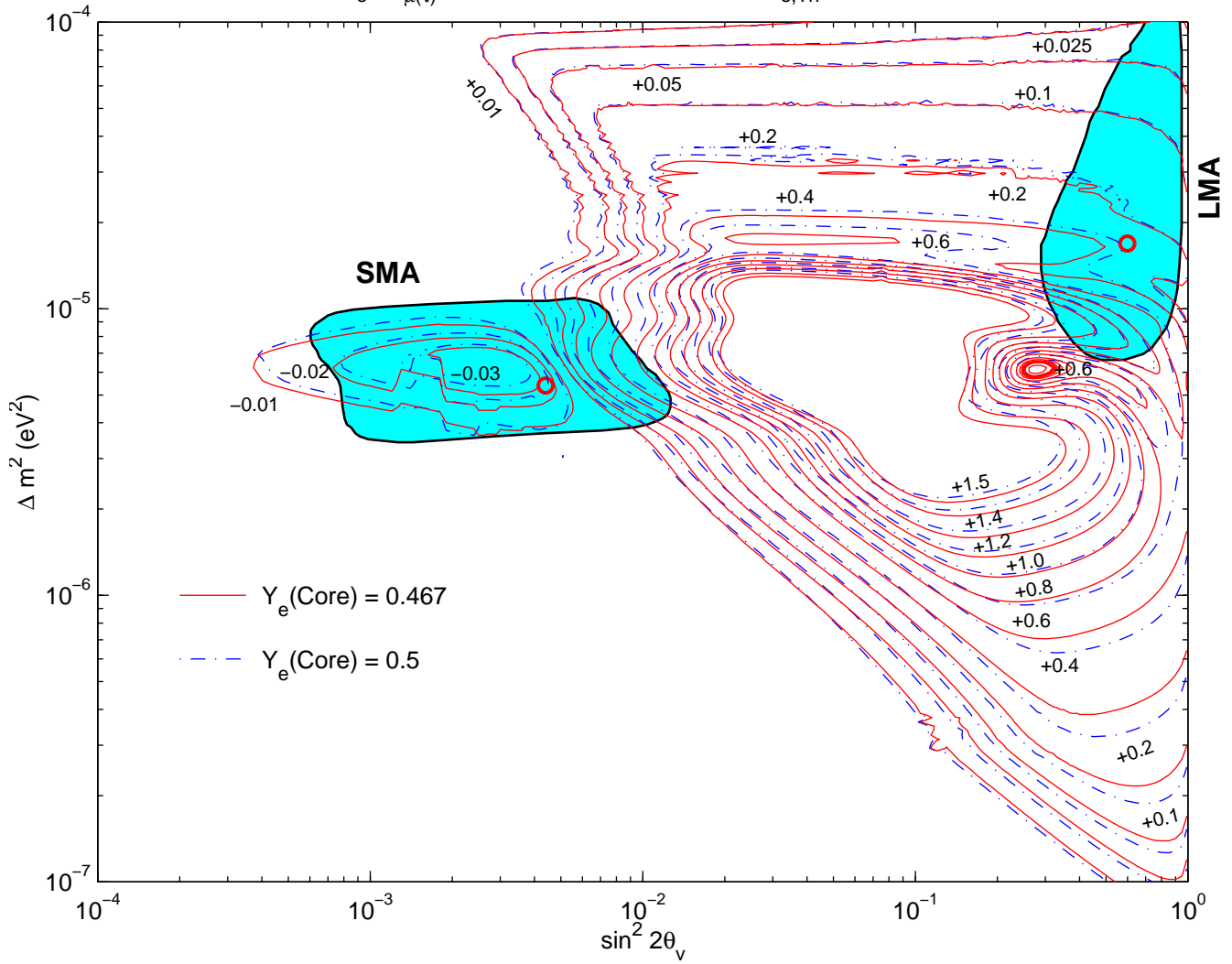
$\nu_e \rightarrow \nu_s$, Core, SNO Charged Current ($T_{e, \text{Th}} = 5.0 \text{ MeV}$)



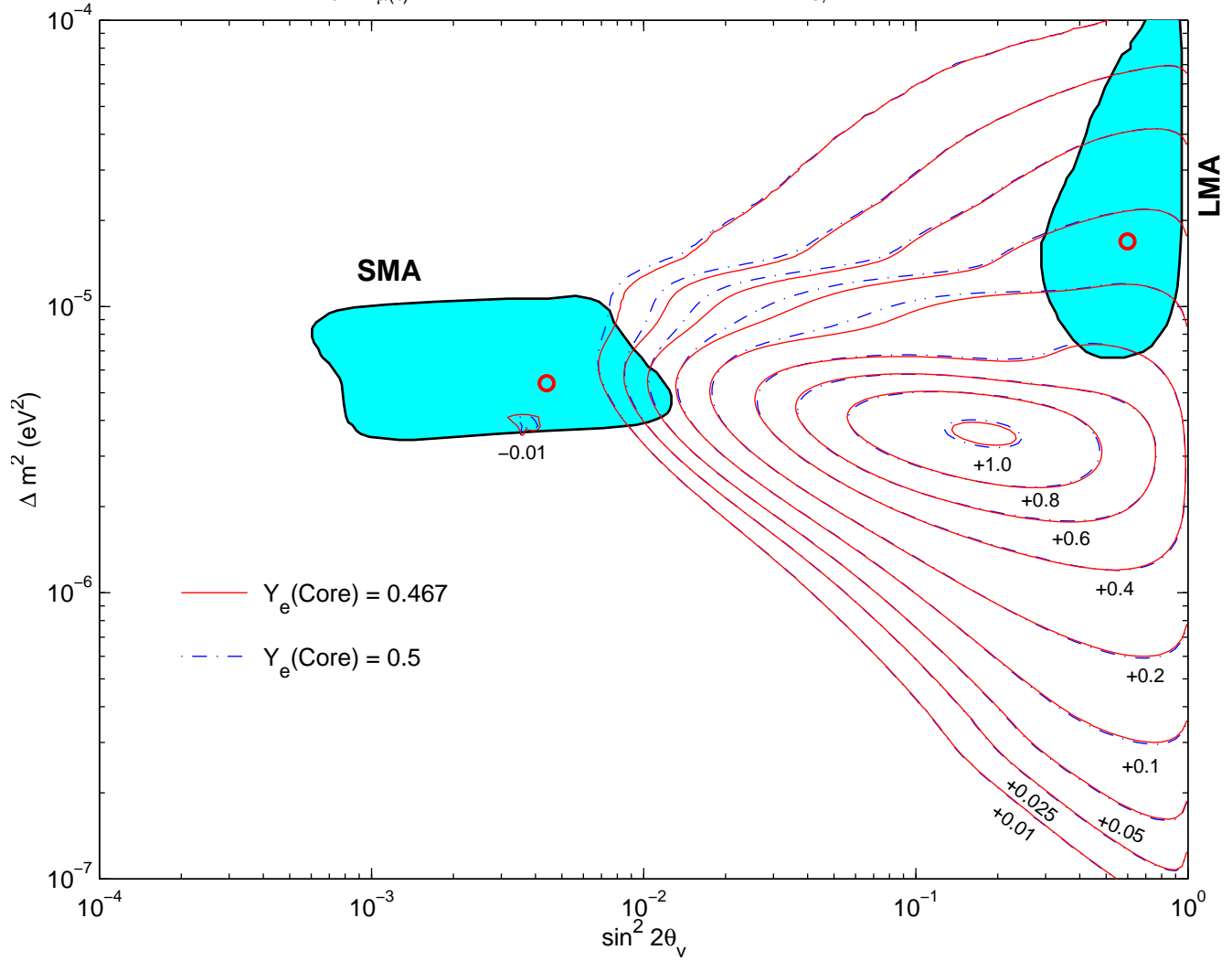
$\nu_e \rightarrow \nu_{\mu(\tau)}$, Full Night, SNO Charged Current ($T_{e, Th} = 7.5$ MeV)



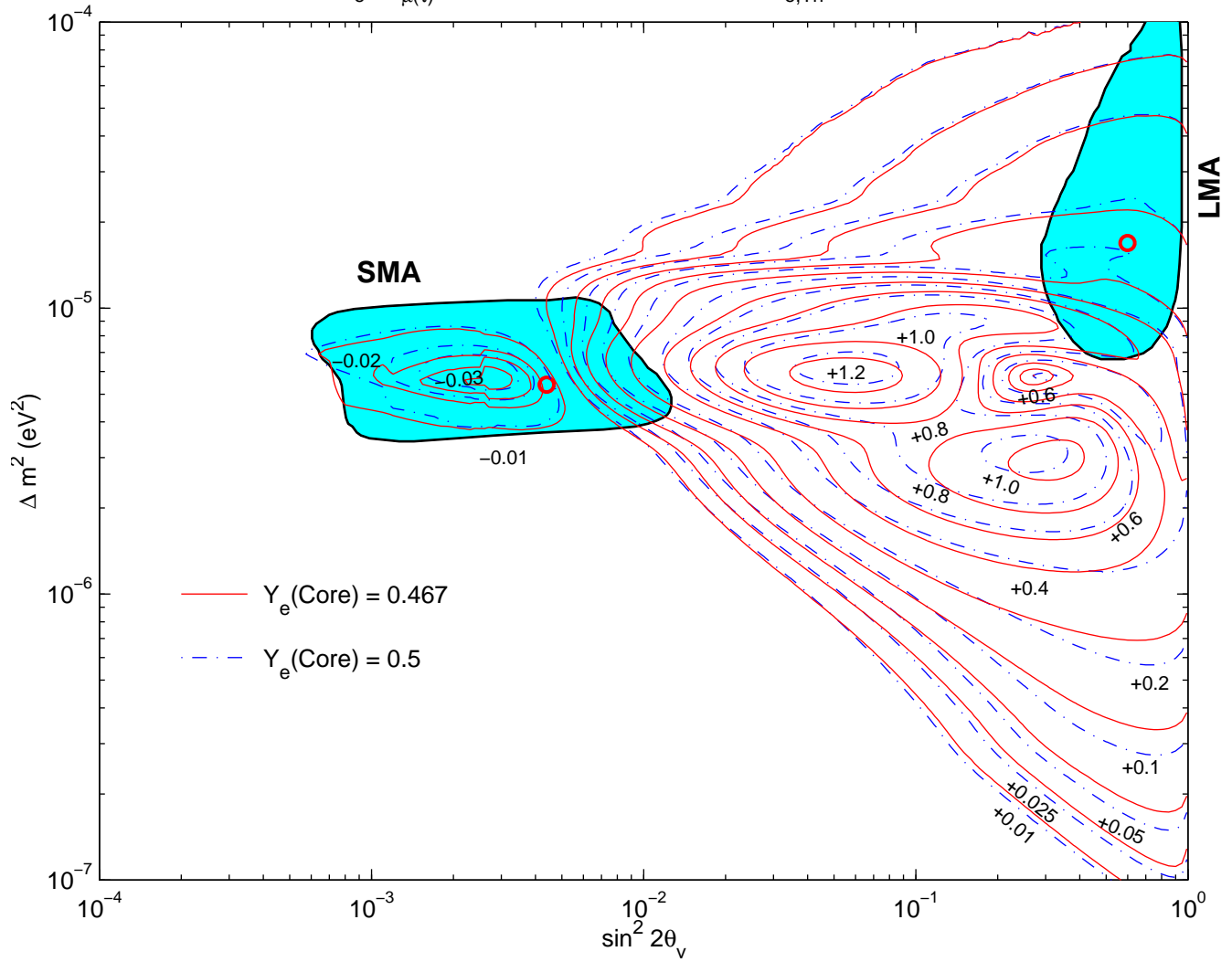
$\nu_e \rightarrow \nu_{\mu(\tau)}$, Core, SNO Charged Current ($T_{e,Th} = 7.5$ MeV)



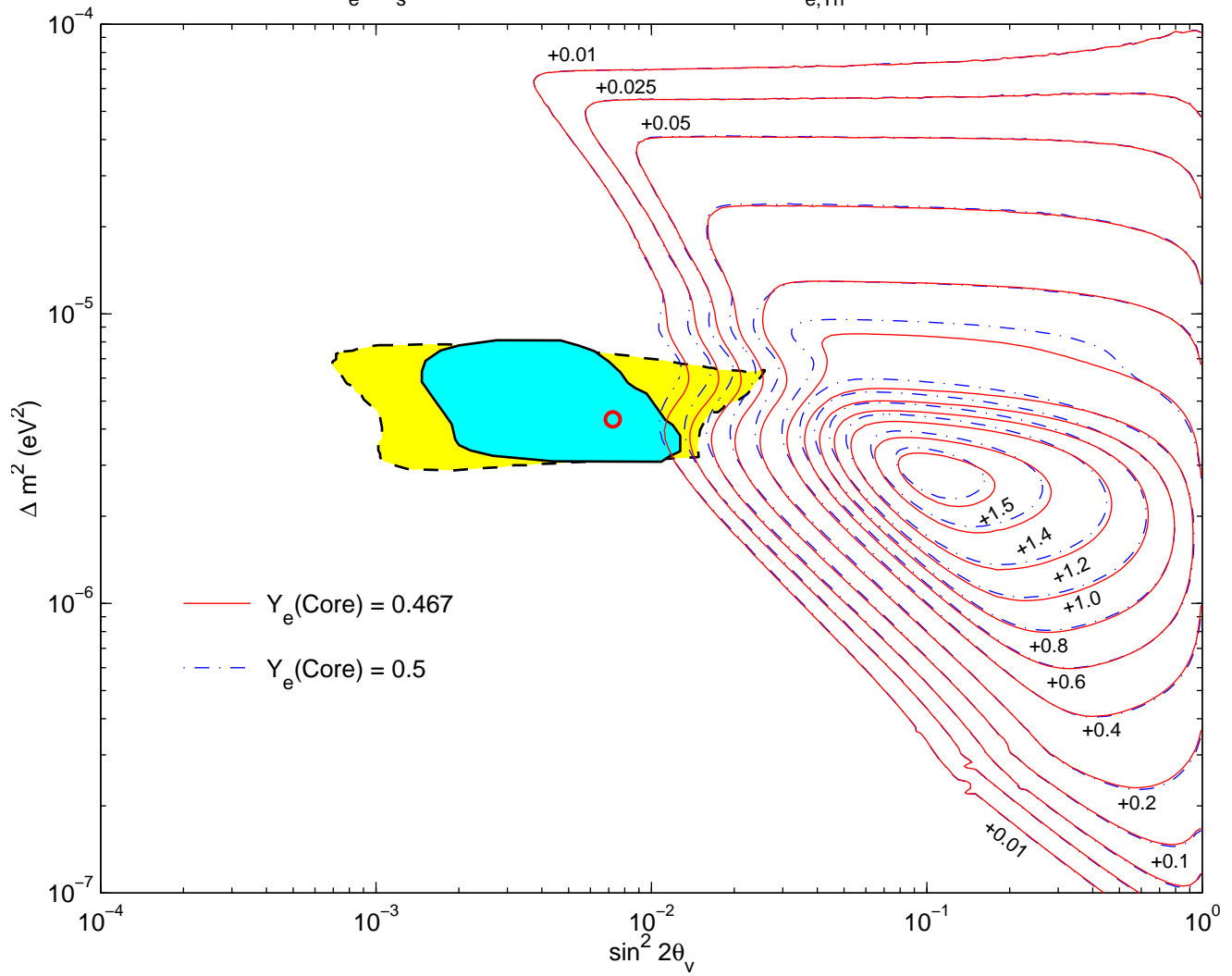
$\nu_e \rightarrow \nu_{\mu(\tau)}$, Full Night, SNO Elastic Scattering ($T_{e,Th} = 7.5$ MeV)



$\nu_e \rightarrow \nu_{\mu(\tau)}$, Core, SNO Elastic Scattering ($T_{e,Th} = 7.5$ MeV)



$\nu_e \rightarrow \nu_s$, Full Night, SNO Charged Current ($T_{e, \text{Th}} = 7.5 \text{ MeV}$)



$\nu_e \rightarrow \nu_s$, Core, SNO Charged Current ($T_{e,Th} = 7.5$ MeV)

